THE CATHOLIC UNIVERSITY OF AMERICA

Artificial Underwater Electrolocation

A DISSERTATION

Submitted to the Faculty of the

Department of Electrical Engineering and Computer Science

School of Engineering

Of The Catholic University of America

In Partial Fulfillment of the Requirements

For the Degree

Doctor of Electrical Engineering

By

Rocco V. Arizzi

Washington, D.C.

2011

Artificial Underwater Electrolocation

Rocco V. Arizzi, PhD.

Director: Dr. Mark Mirotznik, PhD.

Electric Fields can be used as a means of underwater detection, localization and characterization of objects. Observations of certain species of weakly electric fish suggest the possibility of near-field underwater detection capabilities through the use of biologically inspired electrolocation. A system featuring a dipolar electric field source, analogous to the electric discharge organ of weakly electric fish, and an appropriate arrangement of electric potential sensors could emulate this phenomenon. A mathematical model was developed through the method of images to represent canonical spherical targets in the presence of a static, finite, dipolar electric source in a conducting medium. Characteristics of the electropotential pattern on a sensor array are shown through matrix transform models to predictably vary according to the radius, location and material composition of the target spheres. Transform matrices are determined by parameters relating to a given set of physical circumstances. An inverse model follows from the invertible and linear forward model, such that the relevant target characteristics can be gleaned from a given electropotential pattern and appropriate matrices. The accuracy and effective range of predictions for certain practical cases of varying scales and configurations was calculated by comparing realistic noise and sensor parameters to simulation results. Applications to marine littoral environments were explored as they relate to the simulations.

This dissertation by Rocco V. Arizzi fulfills the dissertation requirement for the doctoral degree in Electrical Engineering approved by Dr. Mark Mirotznik, as Director, and Dr. John Holmes, and Dr. Ozlem Kilic as Readers.

_____

Dr. Mark Mirotznik, Director

_____

Dr. John Holmes, Reader

_____

Dr. Ozlem Kilic, Reader

for Dr. Caspar W. Hiatt, III

Table of Contents

List of Figures

List of Tables

List of Symbols

x,y,z	cartesian coordinates	L	Finite dipole length
r,θ	polar coordinates	μ	magnetic permeability
r,θ,ϕ	spherical coordinates	μ_0	permeability of free space
a	sphere radius	$\vec{n}$	normal vector
b_p	waveform maximal slope	ω	frequency
δ_s	electromagnetic skin depth	Φ	electric potential
d	sphere distance	$\breve{\Phi}$	potential perturbation
$\vec{D}$	electric displacement vector	q	electric point charge
ε	electrical permittivity	γ	dielectric contrast
ε_0	permittivity of free space	γ_σ	electrical contrast
$\vec{E}$	electric field vector	ρ	electrical resistivity
E_0	inducing electric field magnitude	$R_{b/E}$	waveform slope-amplitude ratio
E_p	peak magnitude (waveform amplitude)	σ	electrical conductivity
I	electric current magnitude		
$\vec{J}$	current density vector		

Acknowledgements

My sincerest gratitude goes to prof. W.T. Norris of Aston University, U.K. whose prior work and generous help was indispensible in the completion of this dissertation. Thank you also to my advisors and mentors Dr. Mark Mirotznik and Dr. John Holmes, and my readers Dr. Ozlem Kilic and Dr. Scott Mathews for your patience and guidance. Additional thanks to Mark E. Nelson of Northwestern University, and Bruce R. Hood, Donald Pugsley, John Scarzello, and William Wynn of the Naval Surface Warfare Center.

1 Introduction

Man has often found that solutions to the most complicated problems had lied right in front of his eyes, formulated in geologic time in nature's evolutionary laboratory. Scientists and engineers owe much to the natural world for providing both inspiration and intuition for technologies often taken for granted. The wings of birds are ancestors to the modern airfoil, as are the abilities of dolphins to anthropogenic sonar. Even Velcro owes its existence to seed burrs that latch onto passing animals.

When it was discovered that some unique fishes, known as weakly electric fish (WEF), are able to hunt and navigate in virtual blindness using self-produced electric fields, a new realm of biomimetic study emerged. Decades of observation and experimentation revealed that these nocturnal predators can finely locate and characterize nearby objects by measuring disturbances in their surrounding electric fields. This ability is called electrolocation and is confined to only a few species of fresh water fishes.

The potential usefulness of artificial electrolocation to man, and to naval operations in particular, is evidenced by the perpetual need to detect objects or threats in an undersea theater. Marine detection tasks are traditionally handled via sonar. However, when there are limitations due to noise or reflections in shallow water (littoral) regions, or if other factors – such as acoustic stealth or environmental concerns – prevent the deployment of active sonar, an alternative energy source would prove valuable. Furthermore, an electromagnetic-based detection methodology could provide additional insight into target material properties.

Current lines of inquiry into the abilities of weakly electric fish and potential applications stem directly from the biological study of the animals and the mathematical modeling of the electric field interactions within their range of detection. Test platforms have been constructed

that use stochastic methods for achieving electrolocation, and others that use alternating current (AC) spectrum analysis for target characterization. This investigation seeks a novel approach by confining the problem to a static or quasi-static one, and using the method of images to model the field interactions. The method of images allows the model to be viewed as a summation of current sources, providing a flexible mathematical solution that can be easily manipulated to represent a variety of platforms, targets, and layered media.

An electrolocation methodology develops from the new field model and from the results of prior investigations of how WEF determine object properties from measured electric potentials on their skin. The forward model consists of a transformation matrix that maps the distance, radius, and relative electrical contrast of a canonical sphere onto the characteristics of its resulting electric field perturbation. A unique transformation matrix exists for each field interaction model that accounts for various environmental and source constants. The inverse model then follows by matrix manipulation; such that the properties of a given target sphere can be determined by a measured electric field signature.

This chapter describes the motivation behind naval undersea detection, particularly in the marine littoral, and explains how artificial underwater electrolocation can be appropriate as an adjunct or alternative to sonar. The inspiration provided by weakly electric fishes and their singular abilities is explained, as is how those abilities can relate to real-life scenarios. Prior work in underwater electromagnetic (EM) detection and the current state-of-the art in artificial electrolocation are outlined.

Chapter 2 reveals how a method of images formulation of electric fields in conducting media is derived, using duality, from similar formulae for dielectrics. This method is used to

describe the field interactions of conducting spheres in the presence of finite-length point-source current dipoles. It is shown how superposition can be used to describe more complicated sources characterized by multipoles. The fields are plotted to show the electric field interactions for spheres that have conductivities either lower or higher than the surrounding seawater medium.

A forward model is constructed in Chapter 3 from the previously observed relationship between the properties of target objects and the perturbation pattern cast by those objects on a fish's electrosensory array. The relationship is simplified to account for conductive polarity, distance, and radius from the waveform characteristics of a measured electric signature. This relationship is given in matrix algebra form, with transformation matrices giving the signature and its derivatives as functions of the desired sphere properties.

Chapter 4 describes derivation of the inverse model that follows naturally through inversion of the transformation matrices in the forward model. The inverse model allows the sphere properties to be given as functions of the perturbation signature characteristics so that the target location and size can be predicted. Conducting and insulating spheres of varying distance and radius are simulated using finite element method (FEM) software to provide independent input into the inverse model. The accuracy of the electrolocation predictions is then assessed.

Chapter 5 concludes the investigation by first discussing the potential sources of error in the model predictions. The expected detection range for various source configurations is also assessed. Finally, suggestions for future efforts are outlined. Appendix I details the original method of images formulation for dielectric spheres in dielectric media. Appendix II justifies the

use of method of images and duality by comparing their electric field falloff and sphere signatures to those calculated using FEM.

1.1 Motivation: Undersea Detection

The abilities of certain animals to locate prey underwater using electric fields, as well as the proven capabilities of existing EM-based systems, suggest that detection, location, and characterization of objects in a marine environment is practicable. Finding sea mines and other objects of interest, either shallowly buried or "proud" on the seabed, is desirable. Nearby objects or threats in the water such as aquatic animals, human divers, or underwater vehicles would also be detectable.

Aside from object detection, electrolocation could be useful as a navigational aid for undersea vessels. As most relevant barriers are large and differ in conductivity from seawater, they would be detectable by their significant distortion of a background or actively produced field. Because of the rapid falloff of electric fields in seawater, the detection range is short when compared to the more ubiquitous acoustic systems. However, the shorter-range electric fields can be an asset in terms of stealth, since they are less conspicuous in the active mode.

1.1.1 Marine Applications

Among the possible applications of artificial underwater electrolocation is that of detecting targets with a small unmanned underwater vehicle (UUV) within its near-field (a distance on the order of the vehicle's length). An array of sensors in a prolate-spheroidal or cylindrical arrangement on the vehicle surface and accompanying an active electric source would

resemble the source-sensor configuration of the weakly electric fish (as described in section 1.2.2), but on a slightly larger scale. In this case, the detection volume projects radially outward from the vehicle, and extends to either a conduction boundary (such as the water surface or sea floor) or to the limit of the system's detection range for the given source strength and target size.

Due to its size and mobility, a UUV-based electrolocation system could be capable of searching for specific objects by carrying its detection array over areas of interest – much in the way a weakly electric fish hunts for prey in dark, muddy waters, so the vehicle's detection range need not necessarily be much larger than its own length. In the case of detecting sea mines, it is important to note that due consideration must given to the amplitude of the active discharge signal, since many sea mines are designed to detonate upon detection of variation in the electromagnetic field of the surrounding medium (Hartmann 1979). Electrolocation can also be used for autonomous underwater vehicle (AUV) navigation within narrow caverns and provide collision avoidance with respect to other nearby vehicles (Chetty and Russell 1998).

For larger vessels, some uses of an electrolocation system include the detection of nearby threats such as sea mines (again keeping in mind EM conspicuousness) or potentially hostile personnel swimming or diving near the hull. In order to be detected, potential targets need to have an electrical conductivity that differs sufficiently from the surrounding medium, and be large enough to be detected given the electric source strength and sensor resolution. Another possible use of electrolocation for sea vessels is for detection of other nearby vessels or large boundaries in order to avoid collisions. For instance, submarine navigation through caverns or canyons could be aided by such a detection capability when other means are unavailable. If other large vessels are passing nearby or overhead, collision avoidance is crucial.

A stationary underwater electrolocation array would be well suited for detecting large target objects that have a high contrast in electrical conductivity with the medium. Such an arrangement may need to be passive, since a dense array over a large area with a great enough active discharge signal to detect small objects may be prohibitive in terms of cost, installation, and environmental factors. However, natural background fields could induce enough of a response to allow detection of large anomalies (Kraichman 1977). An example of a use of such an array would be for detecting ships passing over a restricted area, a capability that could prove useful for port security (Arizzi 2009).

1.1.2 Comparing Acoustic and Electromagnetic Energy in Seawater

Acoustic waves in seawater experience losses in energy due to geometric spreading, as well as attenuation due to mechanical absorption and scattering. Acoustic propagation in seawater is a complicated problem, affected by water density, temperature, salinity, depth, source frequency, the composition and shape of the sea bottom, and the existence of thermoclines and other layered variations in material properties. In general, acoustic transmission losses can be approximated by adding the geometric spreading losses to those suffered from absorption and scattering. Because of surface and sea bottom reflections, the transmission range of acoustic signals is extended as spherical geometric spreading becomes cylindrical for a bounded medium. Geometric spreading losses for omnidirectional acoustic signal sources are inversely proportional to the square of the distance in a homogeneous medium (Federation of American Scientists 2009).

In comparison to acoustic energy, electric fields attenuate more rapidly in seawater. The field intensity for an electric source attenuates at a rate inversely proportional to the cube of the distance, and more rapidly for multipole sources (NSWCCD Signatures Directorate 2003). The electric permittivity (dielectric constant) of seawater, nominally 80 F/m, and electric conductivity, nominally 4 S/m, contribute to the conduction and ohmic losses that result in attenuation of electromagnetic waves by suppressing the electric field component. Losses in electromagnetic energy, like acoustic waves, are subject to losses due to geometric spreading of the fields through the volume of the medium.

Any comparison of the performance of acoustic and electromagnetic waves in seawater with respect to system design is ambiguous without thorough consideration of the source strength, frequency, environmental noise, material boundaries and sensor capabilities of the respective realizable systems. However, because of their more rapid falloff and their interaction with certain materials, the use of electric fields can serve as a replacement or complement to sonar when the need arises. The high performance of acoustic waves in seawater can come with an accompanying detriment to stealth as well as unwanted distortions due to reflections in the littoral. The capabilities of some fishes to use electric fields for prey capture reveal a potentially powerful alternative for undersea detection.

1.2 Inspiration: Weakly Electric Fish

1.2.1 Sensing in Nature

The pressures of nature, particularly in extreme environments, have resulted in unique adaptations by which some animals sense their surroundings. Both passive and active sensing

modes have developed appropriate to the particular challenges faced by each species. In addition to the five senses (some of which may be useless or absent in certain scenarios), mechanisms that make resourceful use of electromagnetic, mechanical, thermal, and chemical energy exist where the conditions demand (Maciver and Nelson 2006).

Passive sensing

Passive electric and magnetic sensing has evolved in a number of different animals. In a passive mode the animals sense and react to the ambient electric field environment without emitting their own field. Along with the lessened requirement for energy expenditure, a key advantage of passive sensing is reduced conspicuousness. A variety of field gradients are exploited by animals to gain information about their environment. Cave fish, which are completely blind to visible light, are able to detect changes in nearby water pressure with such high fidelity as to effectively characterize nearby objects and fishes. Homing pigeons and other birds, as well as sharks, can follow the magnetic field lines of the earth for precise long-range navigation.

Several types of aquatic animals passively detect low-frequency electric fields through arrays of electric potential sensing cells. This ability is referred to interchangeably as electroreception or electroception. Large catfish, sharks, rays, and billed monotremes (platypus and echidnae) use passive electroreception to varying degrees and purpose. Sharks are known to be the most sensitive creatures to electric fields. Although they emit no electric energy of their own, the platypus and hammerhead sharks achieve a quasi-active mode by sweeping their arrays

(concentrated in the bill and brow, respectively) in a regular motion near an area of interest (Pettigrew 1999).

Active sensing

The use of whiskers and antennae to interact tactilely with the environment is considered active sensing because of the energy expenditure and conspicuousness. The cases in which energy is propagated at a distance through a medium as opposed to through body contact are known as teleceptive sensing modes. During any teleceptive activity, geometric spreading and attenuation losses occur in both the transmission and return signals, in addition to any scattering losses. Thus the active emission must have sufficient magnitude as to overcome these losses to the degree in which returning information can be discerned from the background. As a result, teleceptive animals are considerably more conspicuous than their passive counterparts to those that can sense the particular energy being emitted (Maciver and Nelson 2006).

Cetaceans and bats are well known to emit and receive acoustic energy during echolocation. Bioluminescent animals are also classified as teleceptive. Eels and other electric fishes actively produce an electric background field that augments their electroreceptive capability to achieve electrolocation.

1.2.2 Electrolocation

The ability to produce an active electric field is exclusive to electric fishes and is referred to as electrogeneration (Lissman 1957). Not all electrogenic activity is for the purpose of active sensing. Although electric eels and some catfish can use their self-produced fields as an aid to

locating targets, the primary purpose of their high-voltage discharges is to stun or kill prey. The specific process of electrolocation, however, is exclusive to fishes that combine a weak electric field, known as an electroactive organ discharge (EOD), with a dense array of electropotential sensors (von der Emde 2006).

1.3 Electrolocation in Weakly Electric Fish

1.3.1 History and Biology

Observations of electric fishes and their unique characteristics were recorded as early as the 19th Century. Even before their remarkable abilities were known, Darwin observed of the field-producing organs, "…it is impossible to conceive by what steps these wondrous organs have been produced… their intimate structure closely resembles that of common muscle;" Darwin also noted that electric organs occur in few but disparate species, and conjectured that they arose independently (Darwin 1859). Later, the *gymnarchus niloticus*, a North African fish that was known to be effectively blind due to both the turbidity of its environment and to its underdeveloped eyes, was observed to nonetheless navigate with precision in dark, murky rivers. Further study revealed that electric organs were used for orientation and predation (Lissman 1957).

As shown by some sample species in Figure 1 (Lissman 1957), two independent genetic lines are known to possess weak electric organs: gymnotiformes and mormorids. These two groups of fishes have evolved similar structure and capabilities in parallel, as suspected by Darwin. Although the electric organs of the two orders differ somewhat in their physical nature due to their independent development, their function and operation are notably similar. The very

specialized adaptations of gymnotiformes and mormorids presumably arose in response to the uselessness of vision in their respective environments. Although the former occur exclusively on the African continent, the latter in South America, both groups reside in turbid bodies of fresh water and are largely nocturnal, so vision is usually extraneous.

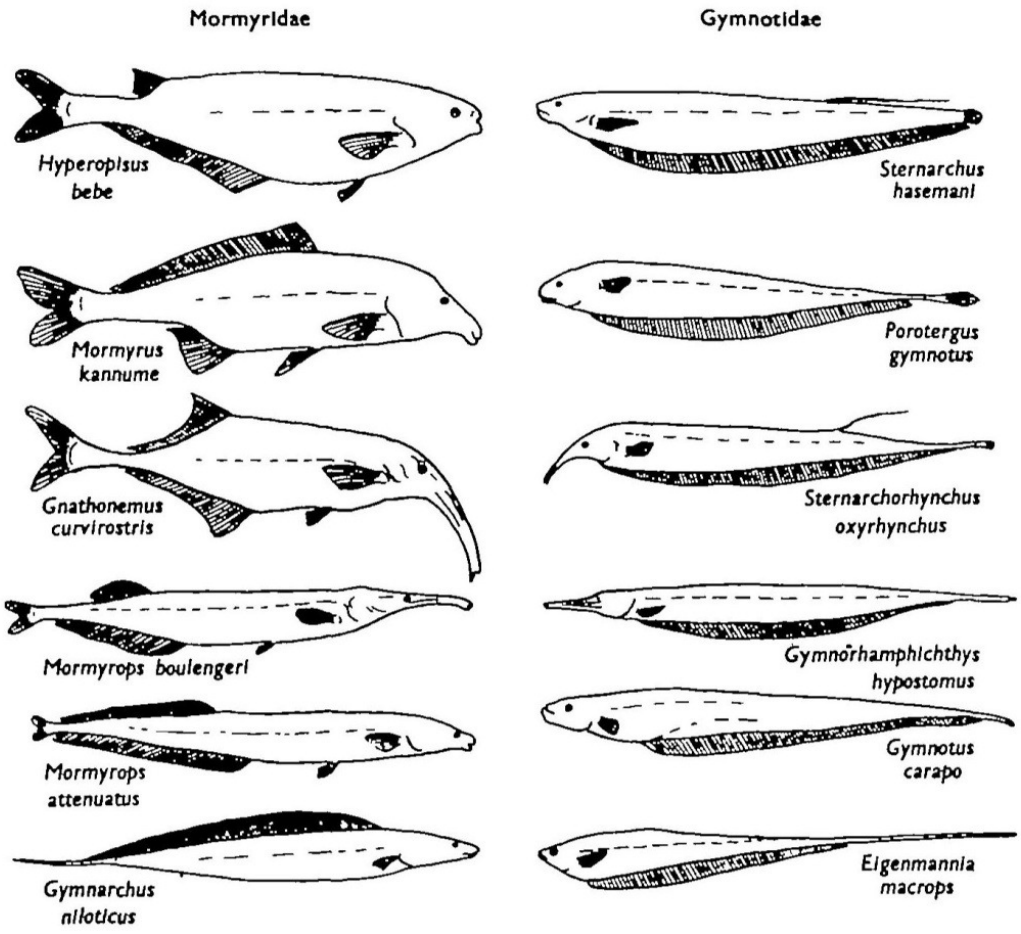

Figure 1 - Select Species in the Two Orders of Weakly Electric Fish

1.3.2 Pulse-type and Wave-type Weakly Electric Fish

With respect to electrolocation, it is more practical and more common to sub-classify individual species by the nature of their EOD instead of their taxonomy. Among both genetic lines there are two types of discharge signals that have been observed, each with their own set of advantages and limitations. Pulse-type fish emit a broadband pulse at regular intervals during electrolocation and wave-type fish produce a quasi-sinusoidal oscillation.

Pulse-type

The pulse duration and inter-pulse intervals of pulse-type WEF vary by species and individual but are generally in the millisecond range, with amplitudes on the order of tens to hundreds of mV/cm. The discharge rate becomes more rapid and regular when the fish is confronted with certain stimuli or is actively engaged in electrolocation, presumably in order to increase the rate at which information is acquired. Some species with more regular pulses are able to modulate their rates in order to avoid confusion with other nearby individuals, but the natural irregularity of the signal tends to prevent this crosstalk and is considered one advantage of pulse modulation (MacIver and Nelson 2001).

Wave-type

Wave-type weakly electric fish produce quasi-sinusoidal electric fields that typically fall in the range of 0.1-10 kHz, again depending on the species and individual, with amplitudes up to 100 mV/cm (Rasnow 1996). The weakly electric fish EOD is one of the most stable oscillators ever observed in nature, and is advantageous to species living in rapid bodies of water where

targets and other cues are constantly in motion and noise is abundant. The regularity of the signal can also, however, be a detriment due to jamming from other nearby individuals, prompting some species to develop a jamming avoidance response in the form of cooperatively shifting EOD frequencies (MacIver and Nelson 2001).

1.3.3 The Active Electrolocation Process

The process of electrolocation by weakly electric fish is an active one, distinguishing it from that of other animals that possess a passive electric sense. There are three principal components that are necessary to achieve electrolocation: an electric source, an electropotential sensor array, and a means of processing the resulting data. Although the parameters vary among the two types and several species of WEF, all individuals feature an electroactive organ for producing fields, a dense array of cells that react to electric potentials on the skin, and a neural network that has evolved to process the perceived electropotential patterns into useful information.

The Electric Source

The electric organs used to produce an EOD consist of a serial battery of individual electrocytes, extending along the lateral line of the fish nominally from the midpoint to the tail (Bass 1986). The result of the discharge is to produce an electric field pattern that, when viewed instantaneously and sufficiently far from the fish body, spatially resembles that of a finite-length dipole. Because of the low frequency of the signals and the related size of typical targets in the environment, the signals can be appropriately viewed as quasi-static in this manner (phase

information has been shown to be useful during electrolocation, but is not in the scope of this dissertation). The electric dipole equipotential pattern, measured in microvolts at an instant in time, produced by a wave-type *apteronotus albifrons* (the "black ghost knifefish") is shown in Figure 2 (Knudsen 1975).

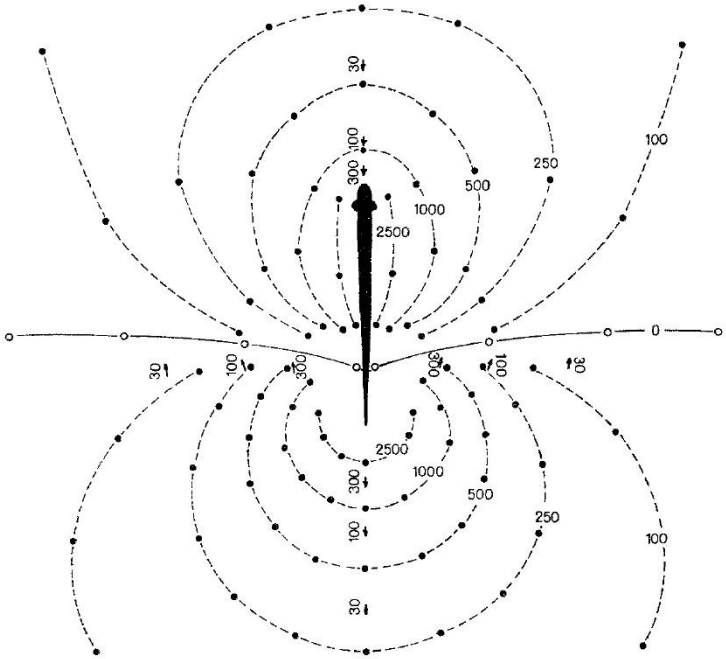

Figure 2 - The Measured Dipole Equipotentials (in μV) of an *Apteronotus Albifrons*

The Sensor Array

The number and distribution of the tubular electroreceptor organs in a WEF are species dependent, but can number in the tens of thousands. Often the sensors are concentrated in denser areas known as fovea. Two types of sensory afferents, P-type and T-type, compose the array of a wave type fish, encoding amplitude and phase, respectively. Phase information seems

to chiefly aid jamming avoidance behaviors as opposed to object detection or prey capture, although phase plays a role in material discrimination. These sensors carry information to other afferent nerve fibers in the fish's electrosensory lateral line (ELL) where processing begins (Heiligenberg 1989). During electrolocation, fish are known to contort their bodies to focus their array on an object or area of interest.

Capabilities

The abilities of weakly electric fish to detect objects and prey in total darkness are well documented. The presence of material that differs in electric conductivity from the medium will cause a distortion in the EOD field that the fish can detect. Objects more conductive than the surrounding water will concentrate electric flux lines where less conductive objects will tend to diffuse them as shown in Figure 3 (Lissman and Machin 1958).

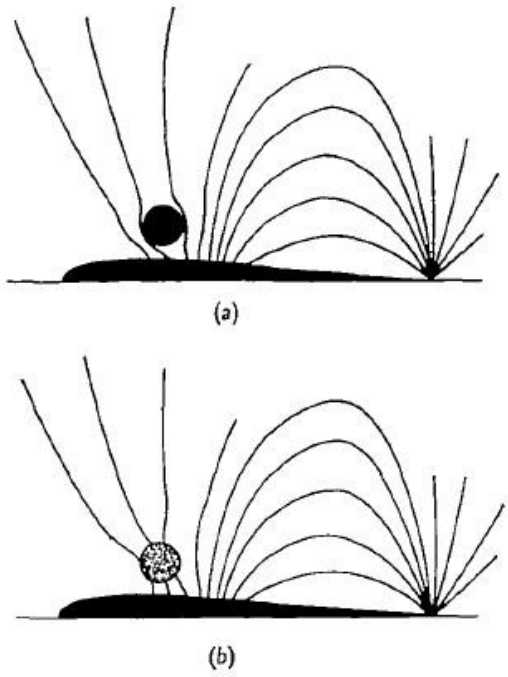

Figure 3 - Distortion of a WEF dipole by (a) a relative insulator (b) a relative conductor

If the disturbance in electric potential is sufficient, it will be detected by the electrorecepters of the WEF and form a distinct sensory pattern or "shadow", known as an electrosensory image, on the fish's sensor array. As seen in the reproduction in Figure 4 (von der Emde and Schwarz 2000), a spherical object will produce an image with an area of peak intensity corresponding to the sphere's center. The location of this peak on the sensor array gives the fish two dimensions of position information about the target. In addition to the location of the image peak, the maximal slope, image width and various waveform distortions provide the fish with sufficient information to determine the object distance, size, conductive polarity and some shape properties.

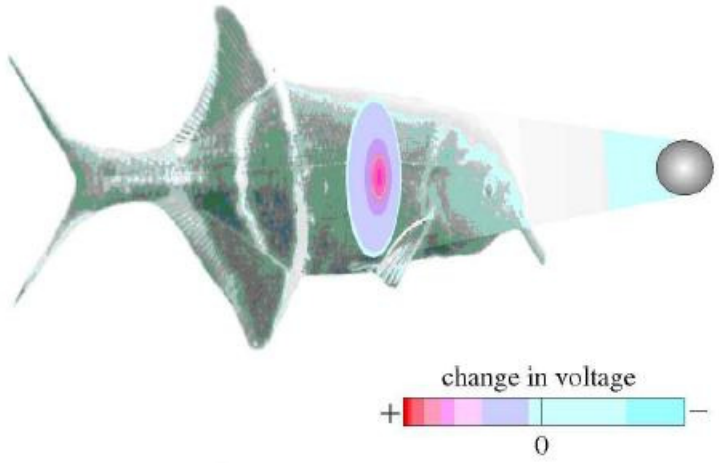

Figure 4 - The Electropotential Image of a Sphere on a WEF

The electrolocation detection range of a fish has been observed to be dependent on the size of the inducing dipole, and is thus proportional to the fish's size. An effective range equal to that of the length of the fish length is an accepted rule-of-thumb. Detectable distortions in the EOD field produced by small prey have been observed to produce disturbances as little as 0.1% of the RMS voltage (MacIver and Nelson 2001).

1.4 Prior and Parallel Work

Once biological research revealed the fascinating and unique capabilities of weakly electric fish, the technological implications were immediately apparent. There are efforts underway to artificially achieve electrolocation, as well as other efforts, past and present, to use electromagnetic energy in general for underwater object detection. Various analytical and numerical models of fish EOD's have been developed as well as hardware prototypes designed to demonstrate the feasibility of artificial electrolocation.

1.4.1 Biorobotic Electrosensory System

Researchers at Northwestern University, who are at the forefront of electrolocation studies, have been developing a laboratory-based electrosensory prototype. The *Electrosenster* is a planar robotic mechanism that features a dipolar electric source coupled with two electric field sensors placed perpendicular to the dipole. The robot carries the arrangement over a shallow pool containing spherical target objects, and uses stochastic methods via a probabilistic control system to analyze field anomalies (Solberg, Lynch and McIver 2008).

1.4.2 Broadband EM Minehunting

Near-field classification of buried sea mines using broadband electromagnetic sensors has been investigated by the US Navy as part of a larger suite of minehunting technologies. Use of electromagnetic induction spectroscopy (EMIS) was shown to characterize metallic objects at short ranges at or under the sea bottom. Co-located source and sensor coils were arranged and tested in a configuration compatible with UUV installation (Purpura, Wynn and Carroll 2004).

1.4.3 Undersea Navigation

Australian researchers, likewise inspired by weakly electric fish, experimented with the use of electric fields for underwater vehicle guidance. Aquatic environments of interest were mapped at close range using impedance image tomography. Images were constructed using inverse transforms of boundary measurement vectors, and revealed regions of impedance that differed from that of the medium (Chetty and Russell 1998).

1.5 Originality

Efforts to mimic the underwater detection capabilities of weakly electric fish must necessarily begin with a sufficiently robust model of the source and target region. Although the electric field pattern of a fish EOD spatially resembles that of a dipole, it is more precisely represented by multipoles (Babineau, Longtin and Lewis 2006). Such would be expected to be the case for any vehicle or apparatus carrying an electrolocation system, since the chassis material and internal parts may contribute to the electric field interactions. This investigation took a novel approach by using the method of images to characterize the model space in terms of point current sources.

The application of the method of images to conducting spheres near point current sources within conducting media was apparently absent from literature, and was approached in this work by applying the principal of duality to existing treatments regarding dielectric spheres. The resulting field model of a point current source and its attendant images in a sphere is a novel and flexible representation that allows for the straightforward modeling, through superposition, of any electrolocation source that can be characterized as an electric multipole. This representation of the model space as a collection of point sources and images provides the additional advantage of allowing the introduction of a multi-layered medium – a useful feature for modeling littoral regions.

There are certain parameters – such as the source strength, source and array configuration, and the electrical conductivity of the medium – that will remain constant during a given electrolocation task. Each unique set of parameters produces a mapping of sphere properties onto the measured field perturbation. The representation of these relationships as a

set of transformation matrices that can be algebraically inverted into a predictive model is an original approach to electrolocation and adds further flexibility to the implementation of a realizable system.

2 Electric Fields in the Presence of a Sphere

The effects of a spherical object on the field produced by a finite-length electric dipole can be determined by considering each pole independently, then superimposing the results. Although this dissertation will be limited to dipolar sources, the use of superposition on single-pole calculations will allow for the modeling of more complicated systems. A real-world electrolocation apparatus can be more accurately represented by a multipole model that accounts for its other material and electronic interactions with the medium in addition to the dipole EOD source.

A multipole representation can be accomplished through superposition, provided that the effects between each pole and a target object are accounted for. This chapter constructs a dipole in this manner by first solving the problem of a point current source near a conducting sphere in a conducting medium using the method of images. It is shown how this point-source approach can be extended to multipole sources and to three-layer conducting media. The behavior of the dipole field near spheres whose conductivities are greater than and less than the surrounding medium (which is chosen to be that of seawater) is described. The assumptions and approximations that were adopted for the electrolocation model are listed.

2.1 The Method of Images

Well-known solutions for electrostatic point charges near dielectric and conducting spheres commonly employ Legendre polynomial expansions to solve Laplace's and Poisson's differential equations (Jackson 1999). These solutions become extremely complicated when considering three dimensions and current sources in conducting media. The method of images is an alternative approach to solving electrostatic problems involving multiple media. This method

eliminates material interfaces and substitutes image charges that are placed so as to produce equivalent field effects in direct application of Gauss' law (Elliott 1999).

In addition to its ease of calculation, the method of images provides a more portable solution that can be further refined to consider reflections in a half-space or three-layer environment. Because many of the intended applications of artificial electrolocation are in the marine littoral, accounting for reflections could achieve a more accurate model. Multi-layer models of electric current point sources in marine littoral environments use the method of images to account for these reflections (Linck 2002). An electrolocation model consisting solely of point sources and their associated images could be adapted to littoral environments in this manner. The theoretical image transformation of a dipole EOD apparatus model near a spherical target in a layered space is shown in Figure 5. Note that the apparatus is replaced by a multipole model and all boundaries are eliminated, leaving nothing but point sources in a medium with properties of the center layer.

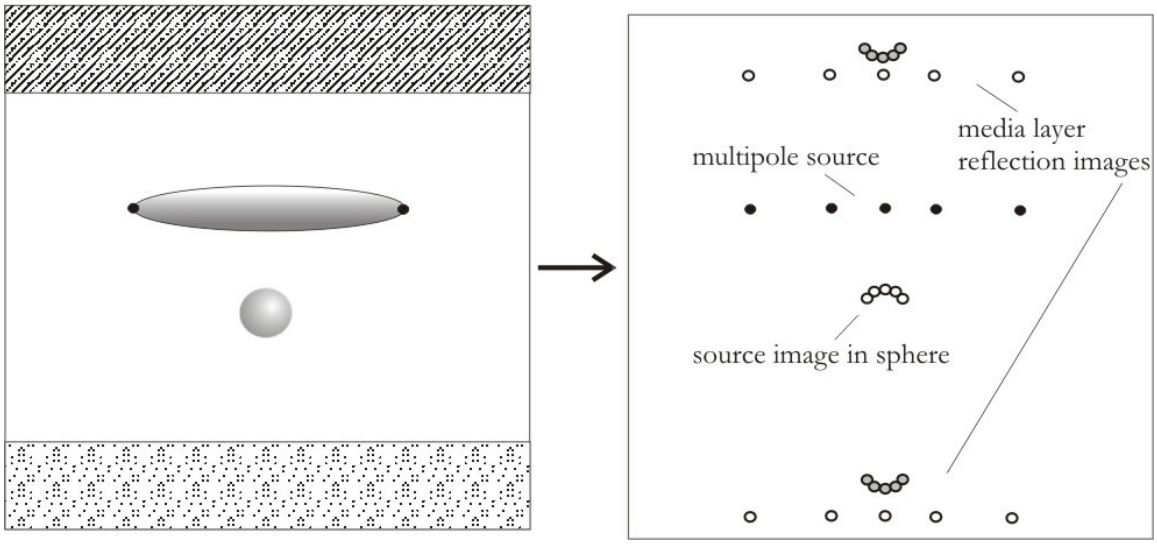

Figure 5 - Transformation of a Three-layer Electrolocation Model via Method of Images

2.1.1 Kelvin Inversion

The simplest application of the method of images involving a sphere was developed by Lord Kelvin and is that of a point charge in free space in the presence of a perfectly conducting sphere. The method of images is predicated on the notion that two point sources of opposite charge will give rise to equipotential surfaces in the intermediate space. If the two charges are equal in magnitude, there exists a planar surface whose potential is zero, and thus is analogous to the boundary between a conductor and free space. However, two charges of unequal magnitude and opposite polarity will produce a zero-potential surface that is a sphere encompassing one of the charges.

Consider the perfectly conducting sphere of radius a near the point charge q illustrated in Figure 6. Assume the external medium to be free space and the point charge is a distance r_s from the sphere center. According to the method of images, if an image charge of magnitude q_i is placed collinear to the origin and the point charge q at a distance r_i, given by the equations

below, the resulting magnetic field outside the spherical cavity will be equivalent to that produced by the conductor (Elliott 1999). The procedure of locating an image point charge is historically known as Kelvin inversion.

$$q_i = -q\frac{a}{r_s} \tag{1}$$

$$r_i = \frac{a}{r_s} \tag{2}$$

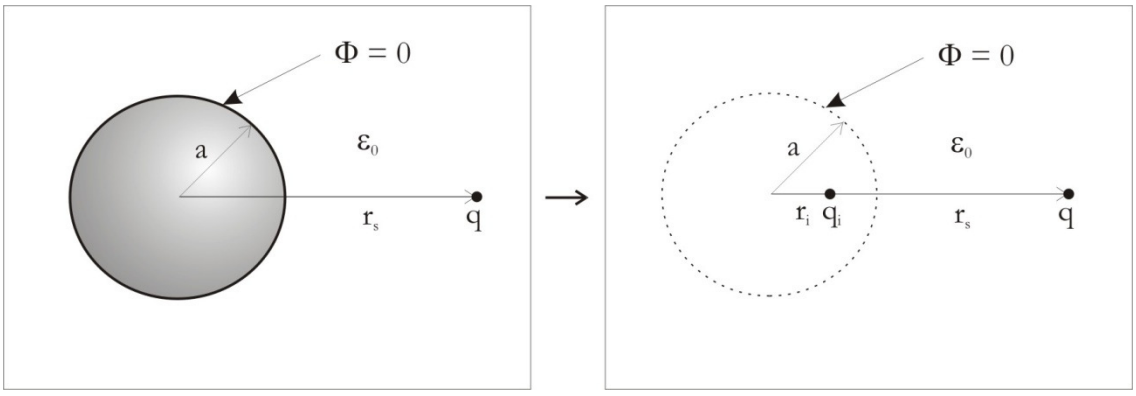

Figure 6 - Kelvin Inversion in a Conducting Sphere

2.1.2 Dielectric Sphere and Medium

A more complicated situation arises when a point charge is placed near a dielectric sphere within a dielectric medium. A non-zero potential is induced within the sphere and on its surface, thus a single Kelvin image is no longer sufficient for describing the resultant fields. A second image, in the form of a distributed line charge, is necessary to complete the transformation (W. Norris 1995). Consider, again, in Figure 7 a sphere of radius *a* near a point

charge q a distance r_s from the origin along the x axis. The electric permittivities of the external medium and sphere are ε_1 and ε_2, respectively.

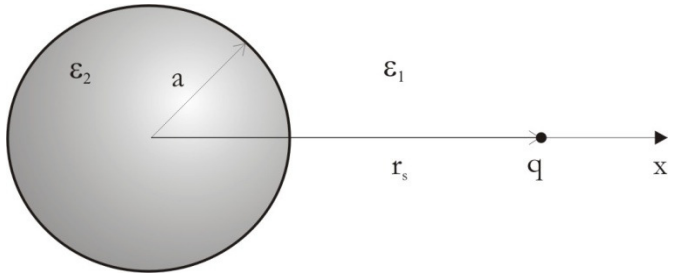

Figure 7 - A Dielectric Sphere in a Dielectric Medium near a Point Charge

Since this is not a free space problem, the dielectric contrast must be considered and is defined as

$$\gamma = \frac{\varepsilon_2 - \varepsilon_1}{\varepsilon_2 + \varepsilon_1}; -1 \leq \gamma \leq 1 \tag{3}$$

The magnitude and position of the Kelvin image then become

$$q_i = \gamma q \frac{a}{r_s} \tag{4}$$

$$r_i = \frac{a^2}{r_s} \tag{5}$$

The distributed line image extends from the origin to the Kelvin image point. The magnitude in terms of x is given by (W. Norris 1995)

$$q_d(x) = \frac{q}{a}\frac{\gamma(1-\gamma)}{2}\left(\frac{r_s x}{a^2}\right)^{-(1+\gamma)/2} ; 0 \leq x \leq a^2/r_s \tag{6}$$

These calculations allow a transformation to the arrangement depicted in Figure 8, where the boundary and internal electric permittivity are disregarded and replaced by the image charges. It is important to note that any field calculations made using the above equations are only valid for the region external to the original sphere; additional equations are needed to determine the field inside the sphere if needed.

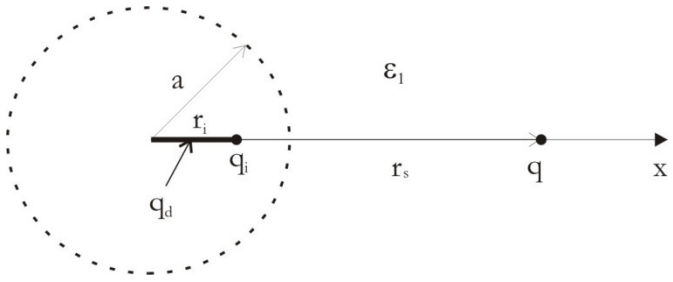

Figure 8 - Transformation of a Dielectric Sphere into Image Charges

The perturbation in electric potential (derivation in Appendix I) at a point in space outside the sphere at a distance r_m from the origin and angle θ to the x axis is given by (W. T. Norris 2010)

$$\breve{\Phi}_{\varepsilon} = \frac{q\gamma}{4\pi\varepsilon_0\varepsilon_1}\frac{1}{a}\int_0^{r_i} \frac{r_i\left(\frac{x}{r_i}\right)^{(1-\gamma)/2}(x - r\cos\theta)}{(r^2 + x^2 - 2rx\cos\theta)^{3/2}}dx\,;x > a \tag{7}$$

$$\breve{\Phi} \stackrel{\text{def}}{\equiv} \Phi_T - \Phi_S$$

2.1.3 Application of Duality

In order to achieve a model for artificial underwater electrolocation, the relative conductivity of the target with respect to the medium must be considered. The method of images as applied to dielectrics can be modified to this purpose using the principle of duality. Duality states that if two systems of equations are identical in form, then the corresponding constants and variables are interchangeable (Paris and Hurd 1969). The following equations defining constitutive relations and tangential boundary conditions for electric displacement *D* and current density *J* are part of a dual set:

$$\begin{array}{cc} \vec{D} = \varepsilon\vec{E} & \vec{J} = \sigma\vec{E} \\ \vec{n}\times\left(\frac{\vec{D}_2}{\varepsilon_2} - \frac{\vec{D}_1}{\varepsilon_1}\right) & \vec{n}\times\left(\frac{\vec{J}_2}{\sigma_2} - \frac{\vec{J}_1}{\sigma_1}\right) \end{array} \tag{8}$$

A direct implication of duality is that any valid equations derived from one form of the set will still be valid if the corresponding components are interchanged. Further, Poisson's equation has the following dual relation (Bronzino 1999)

$$\nabla^2\Phi = \frac{\nabla \cdot \vec{J}}{\sigma} = -\frac{\mathrm{I}}{\sigma} \qquad \nabla^2\Phi = -\frac{\rho}{\varepsilon} \tag{9}$$

where I is current and ρ is charge density. The equation calculating the potential due to a point charge near a dielectric sphere in a dielectric medium (equation (7)) is derived ultimately from fundamental relations in the sets shown in equation set (8), and is thus subject to duality itself. Assuming that the charge density ρ in equation (9) is infinitesimal, it can be treated as a point charge, *q*, in accordance with Gauss's law. The following duality transformations, resulting in the new problem shown in Figure 9, can therefore be made

$$\begin{aligned} \varepsilon &\Leftrightarrow \sigma \\ q &\Leftrightarrow I \end{aligned} \tag{10}$$

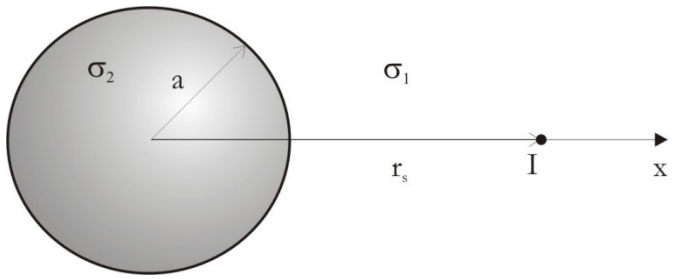

Figure 9 - A Conducting Sphere in a Conducting Medium near a Point Current Source

where I represents a point source of electric current and σ_1 and σ_2 are the electrical conductivities of the medium and sphere, respectively. The dielectric contrast in equation (6) can now be redefined as the electric contrast, γ_σ to account for the difference in conductivity of an electrolocation target from the medium

$$\gamma_\sigma = \frac{\sigma_2 - \sigma_1}{\sigma_2 + \sigma_1}; -1 \leq \gamma \leq 1 \tag{11}$$

Applying the transformation yields new equations describing the image source magnitudes (position is unaffected) as shown in Figure 10

$$I_i = \gamma I \frac{a}{r_s} \tag{12}$$

$$I_d(x) = \frac{I}{a}\frac{\gamma(1-\gamma)}{2}\left(\frac{r_s x}{a^2}\right)^{-(1+\gamma)/2}; 0 \leq x \leq a^2/r_s \tag{13}$$

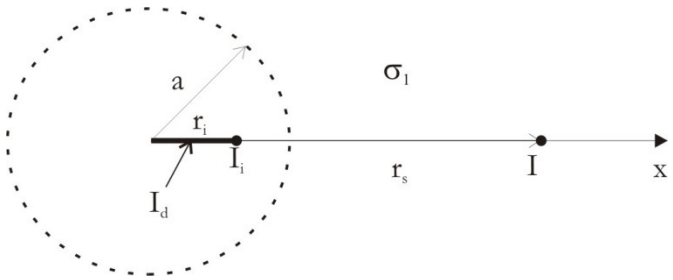

Figure 10 - Transformation of a Conducting Sphere into Image Charges

where I_i is the Kelvin images magnitude and I_d is the distributed current image magnitude with respect to x. Finally, the electric potential perturbation due to a point source of current in a conducting medium near a conducting sphere becomes

$$\breve{\Phi}_\sigma = \frac{I\gamma_\sigma}{4\pi\sigma_1}\frac{1}{a}\int_0^{r_i} \frac{r_i\left(\frac{x}{r_i}\right)^{(1-\gamma_\sigma)/2}(x - r\cos\theta)}{(r^2 + x^2 - 2rx\cos\theta)^{3/2}}dx\,;x > a \tag{14}$$

This equation, based on the aforementioned formulation for point charges in dielectrics, is a unique representation of point current sources near conducting spheres in conducting media, and is the basis of the electrolocation model developed in this work.

2.1.4 Dipole Image by Superposition

A finite-length static electric dipole consists simply of two point current sources of opposite polarity. The method of images can be applied to the sphere and dipole source and the results superimposed as shown in Figure 11.

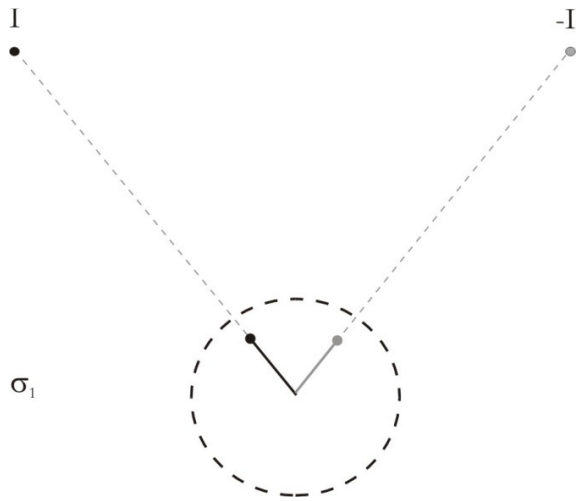

Figure 11 - Image of a Finite Dipole Reflected Across the Boundary of a Sphere

The total potential outside the sphere, Φ, is simply the sum of the potentials, each as formulated in equation (14), Φ_1 and Φ_2 due to the poles

$$\breve{\Phi} = \breve{\Phi}_1 + \breve{\Phi}_2 \tag{15}$$

Similarly, if the static electric signature of the electrolocation apparatus can be represented as a multipole as illustrated in Figure 5 and Figure 12, then the total potential is the sum of individual potentials due to all poles

$$\breve{\Phi} = \sum_{1}^{n} \breve{\Phi}_n \tag{16}$$

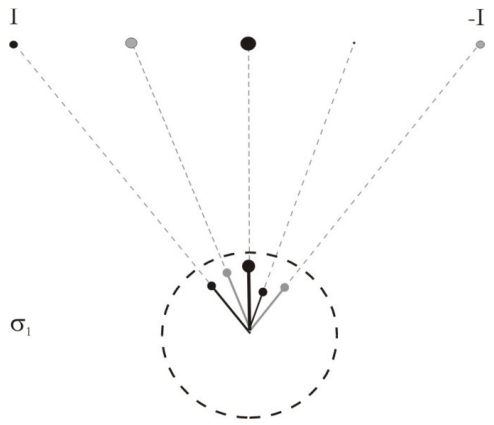

Figure 12 - Image of a Multipole in a Sphere

2.2 Electric Field Calculations

2.2.1 Electric Field Perturbation

The electric field intensity (V/m) is a vector given by the negative gradient of electric potential (Jackson 1999)

$$\vec{E} = -\nabla\Phi = \mathrm{E_x}\vec{\mathrm{x}} + \mathrm{E_y}\vec{\mathrm{y}} + \mathrm{E_z}\vec{\mathrm{z}} \tag{17}$$

where $< \vec{\mathrm{x}}, \vec{\mathrm{y}}, \vec{\mathrm{z}} >$ are the Cartesian unit vectors. The magnitudes of the total electric field perturbation and associated Cartesian components from the potential given in equation 14 are thus

$$\breve{E} = \left|-\nabla\breve{\Phi}_\sigma\right| \Rightarrow (\breve{\mathrm{E}}_\mathrm{x}, \breve{\mathrm{E}}_\mathrm{y}, \breve{\mathrm{E}}_\mathrm{z}) \tag{18}$$

2.2.2 Equipotentials and Field Lines

Before the potential perturbation of a target object can be ascertained, the nature of the active or background field must be established. Using duality to confirm the well-known formula for a finite current dipole in conducting media (see Appendix II) we have

$$\Phi = \frac{1}{4\pi\sigma}\frac{I}{|\vec{r}|} \tag{19}$$

Superimposing the effects of two idealized current point sources of opposite polarity separated by a finite distance yields a dipole analogous to the weakly electric fish EOD. Figure 13 shows the equipotential lines and electric field vectors due to a 1 m dipole with ± 10 A DC current in a medium of 4 S/m conductivity. The lower plot shows more field detail in the area near the origin with a dashed line where a sphere will be placed.

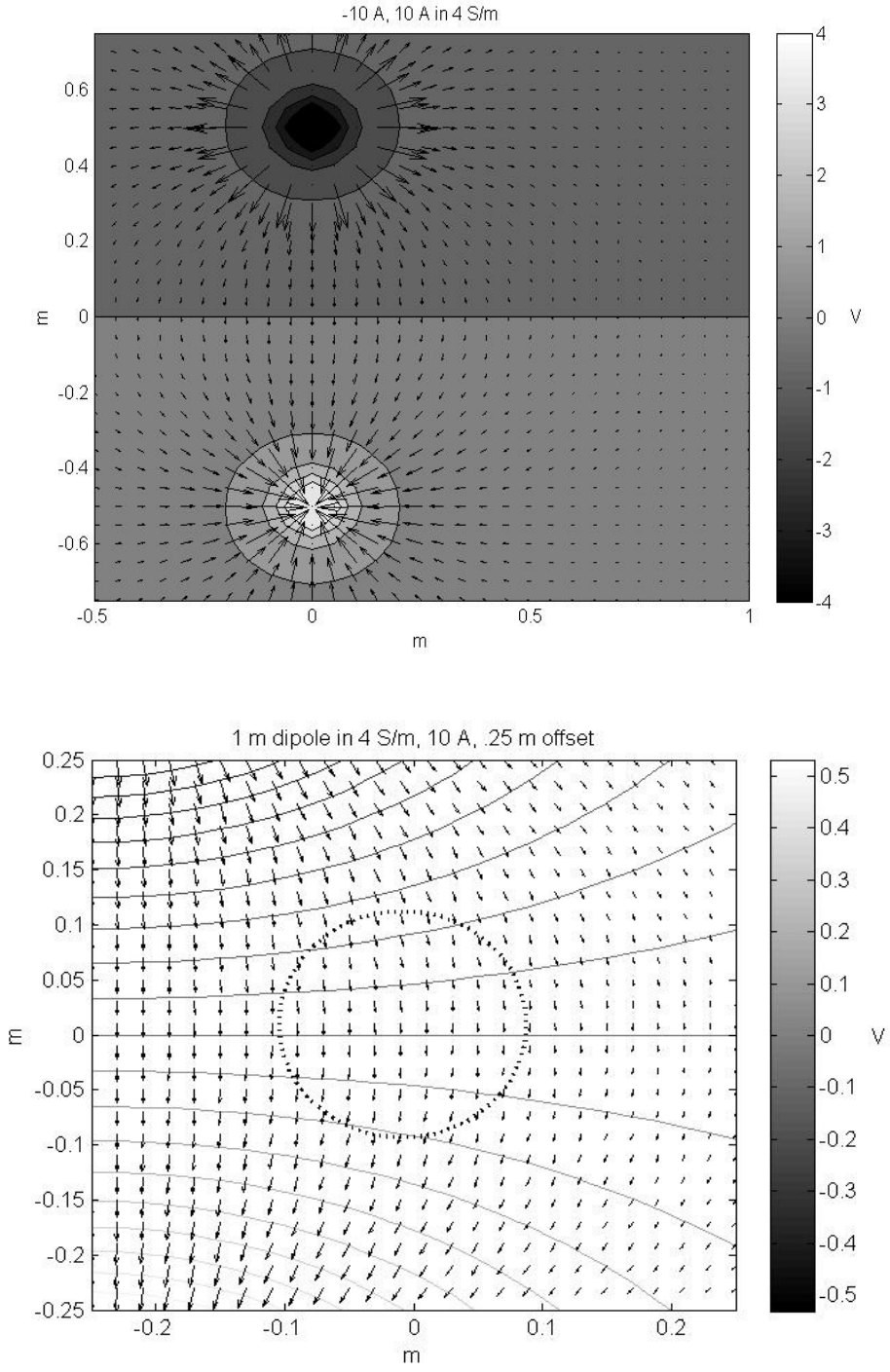

Figure 13 - Equipotential and Electric Field of a Finite Dipole in a Conducting Medium

When a sphere of sufficient electrical contrast to the medium is placed near the dipole source, the fields will be distorted. Figure 14 shows the effect, as calculated using the potential

formula in section 2.1.3 ((14), of a 0.1 m diameter sphere with a conductivity of 1×10^5 S/m placed 0.25 m from the center of the 10 A source from Figure 13. Note that the field vectors concentrate into the sphere and the equipotential lines are diffused.

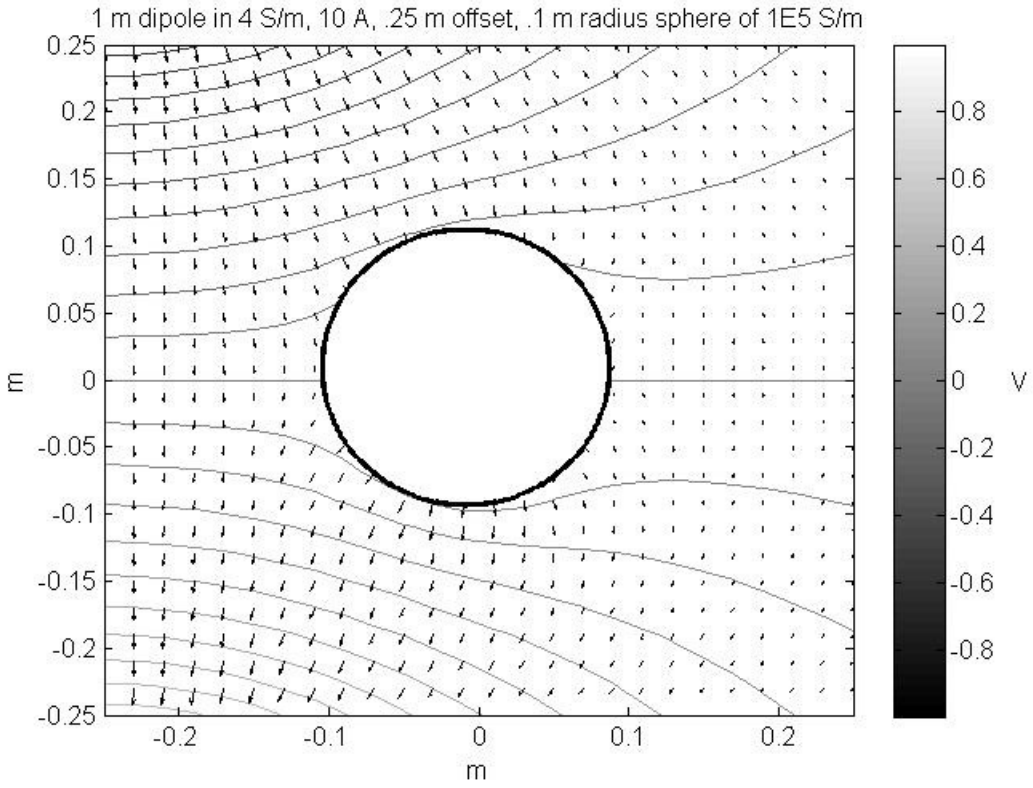

Figure 14 - Equipotentials and Electric Field near a Conducting Sphere

In Figure 15, a 0.1 m diameter sphere with a conductivity of 1×10^{-5} S/m placed 0.25 m from the center of the same source. In contrast to the conducting sphere, the equipotential lines are concentrated near the sphere and the electric field vectors are repelled.

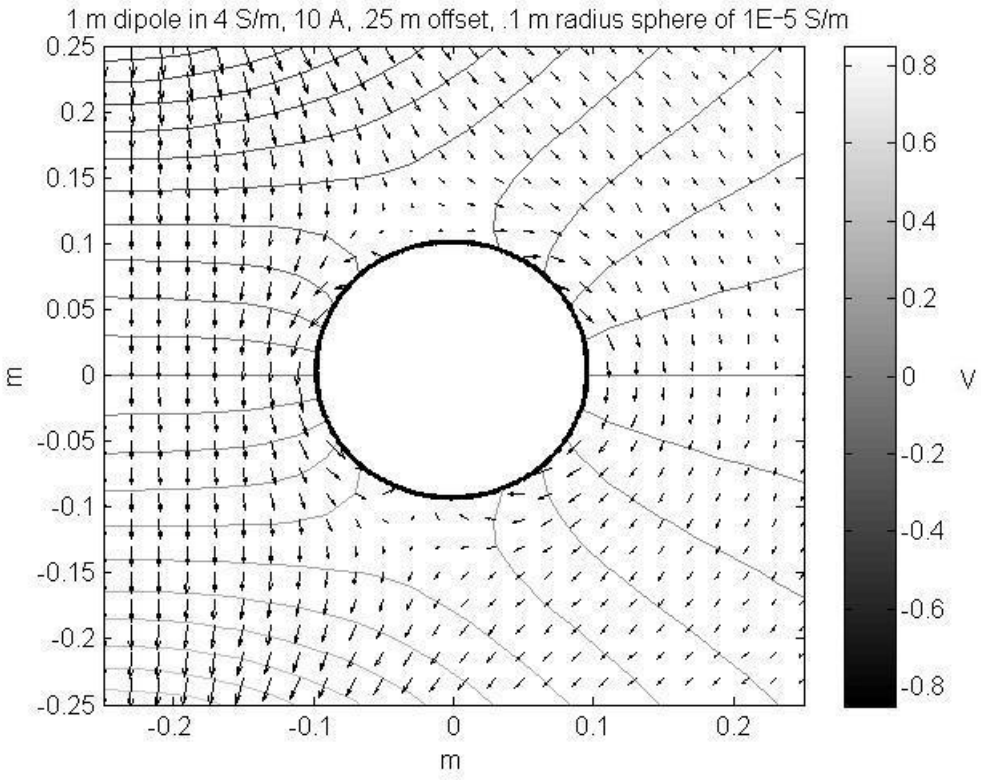

Figure 15 - Equipotentials and Electric Field near a Dielectric Sphere

2.3 Assumptions and Approximations

It has been established that electrolocation occurs in nature over a variety of EOD frequencies and waveforms for different species. It is clear that phase information is useful to wave-type electric fishes in obtaining material information, but that the chief advantage of the oscillating signal is to reduce cross-talk among individuals. Distance, size, location, and conductive polarity of targets can be determined when constrained to a static EOD and is the focus of this work. The chosen model consists of a finite-length dipolar electric current source in an infinite electrically conducting medium, with targets represented by spheres of varying

location, radius, and electrical polarity. Variation of target sphere properties is performed relative to fixed source and medium characteristics.

The model described herein is constructed on the basis of several assumptions intended to establish a basic artificial underwater electrolocation paradigm from which useful systems could be realized. Although active biological electrolocation is only known to occur in fresh water (although decidedly conductive due to its turbidity), the intended and likely application of artificial systems is chiefly in marine environments. The conductivity of the medium is thus held constant at a nominal seawater value of 4.0 S/m. It is important to note that higher values of medium conductivity do affect a more rapid falloff of electric fields, requiring higher EOD amplitude to compensate. This must be considered along with the signal-to-noise ratio of sensor equipment when determining suitable source strength.

Research is still ongoing as to how weakly electric fish use phase information to discern organic matter and living organisms from the environment by detecting complex impedances. In order to maintain a static source that is compatible with the method of images solution (section 2.1), such material was excluded from this model. It is shown in section 3.2 that beyond a narrow band of conductivities near that of the medium there is minimal variation in field for large changes in target conductivity. Given that most metallic objects of interest have a very high conductivity and that insulating objects have a conductivity approaching zero, conductivities of 1×10^5 S/m and 1×10^{-5} S/m were assumed for conductive and insulating targets, respectively.

The image cast by an object on a fish's electrosensory array produces a center-surround pattern representing the electric field perturbation. As seen in Figure 4, this pattern has axial

symmetry for objects with regular or symmetrical profiles. As such, for simplicity, the measurement points lie on a one-dimensional linear array extending parallel to the dipole source, at a length equal to the source. The line is offset a distance equal to one tenth the length of the source on a plane containing the target center. This offset was chosen to represent an arbitrary estimate of a nominal placement of sensors on the hull of an apparatus or vehicle.

Figure 16 is a basic illustration of the assumptions and arrangement of the model. The electric dipole source is represented by two point current sources of opposite polarity, $\pm I$. The sphere of radius a and electrical conductivity σ_2 is centered at the origin of an orthogonal coordinate system. A vector of length r points to the position of measurement, which must be outside the sphere in the medium of electrical conductivity σ_1. The line of measurement is offset a distance of 1/10 the dipole length L in the plane containing the dipole and sphere center.

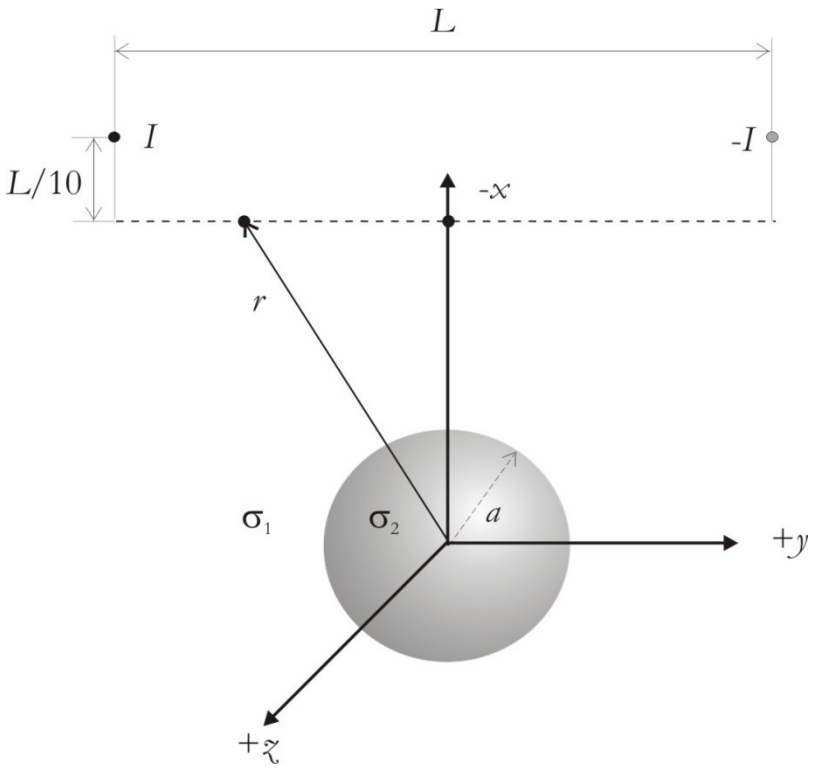

Figure 16 - Artificial Electrolocation Model

The forward model introduced in the following chapter proceeds from the above assumptions. A set of constant parameters are chosen to represent a particular dipole source strength and size in a homogeneous medium. The sphere properties are then varied in order to determine their relationship to the measured electric signature.

3 Forward Electrolocation Model

The method of images applied in the previous chapter served to establish a representation of the electrolocation space that is flexible and adaptable to various scenarios. For a given environment, medium, and apparatus there will be a unique relationship between the properties of a target object and its measured electric signature. Thus a forward model can be established for a given scenario describing this relationship in useful mathematical terms.

Based on prior experiments and observations of weakly electric fish, a relationship between the desired sphere properties and the characteristics of the attendant electric signature waveform is established in this chapter. The mathematical relationship is constructed in matrix algebraic form, giving added flexibility to the model and setting up a simple solution for the inverse model.

3.1 Previous Experimental Observations

Since the discovery of weakly electric fish capabilities, numerous experiments have been conducted in order to discover the manner by which the fish determine object properties. Often, fish were presented with objects of varying size, shape, location and material and rewarded with food upon successful recognition (von der Emde and Schwarz 2000). These procedures, along with analytical and numerical modeling of the fish and experimental environment, produced several hypotheses as to how the properties of target objects are determined from their associated electropotential patterns.

3.1.1 Field Approximation

Since the instantaneous electric field surrounding a WEF resembles a dipole, well known equations can be applied to approximately represent the background field used during electrolocation. Since the medium has a measurable conductance, a finite-length electric dipole source is necessarily represented as a current point source with an associated sink.

If the target object is assumed to be much smaller than, or distant from, the dipole source, the source can be assumed as a uniform field, simplifying the calculation of field interactions. From (Rasnow 1996) the potential perturbation $\breve{\Phi}$ in a uniform electric field of intensity E_0, due to a sphere of radius *a* is given by

$$\breve{\Phi}(\vec{r}) = \vec{E}_0 \cdot \vec{r} \left(\frac{a}{r}\right)^3 \frac{\rho_1 - \rho_2 + i\omega\rho_1\rho_2(\varepsilon_2 - \varepsilon_1)}{2\rho_1 + \rho_2 + i\omega\rho_1\rho_2(2\varepsilon_2 + \varepsilon_1)} \tag{20}$$

where ρ_1 and ρ_2 give the resistivity of the medium and sphere, respectively, ε_1 and ε_2 are the electric permittivities, ω is the field frequency and the measurement position is represented by the vector $\vec{r}$. Note that frequency information is considered in this formula, but that it does not account for the spatial aspects of a finite dipole EOD.

3.1.2 Electropotential Pattern

The image cast on the WEF electroreceptor array (referred to herein as the electropotential pattern to avoid confusion with method of images terminology) by a sufficiently contrasting object with a nominally regular profile is a center-peak formation with a surrounding ridge of opposite polarity. This is often referred to as a "Mexican hat" surface and can be

visualized from Figure 4. The cross section shown in Figure 17 illustrates the behavior of the rostrocaudal (E_y) component of the electric field perturbation parallel to the dipole source on a line between the source and target. The polarity of the center peak and the smaller ridge peaks will depend on the polarity of the electrical contrast between the medium and target.

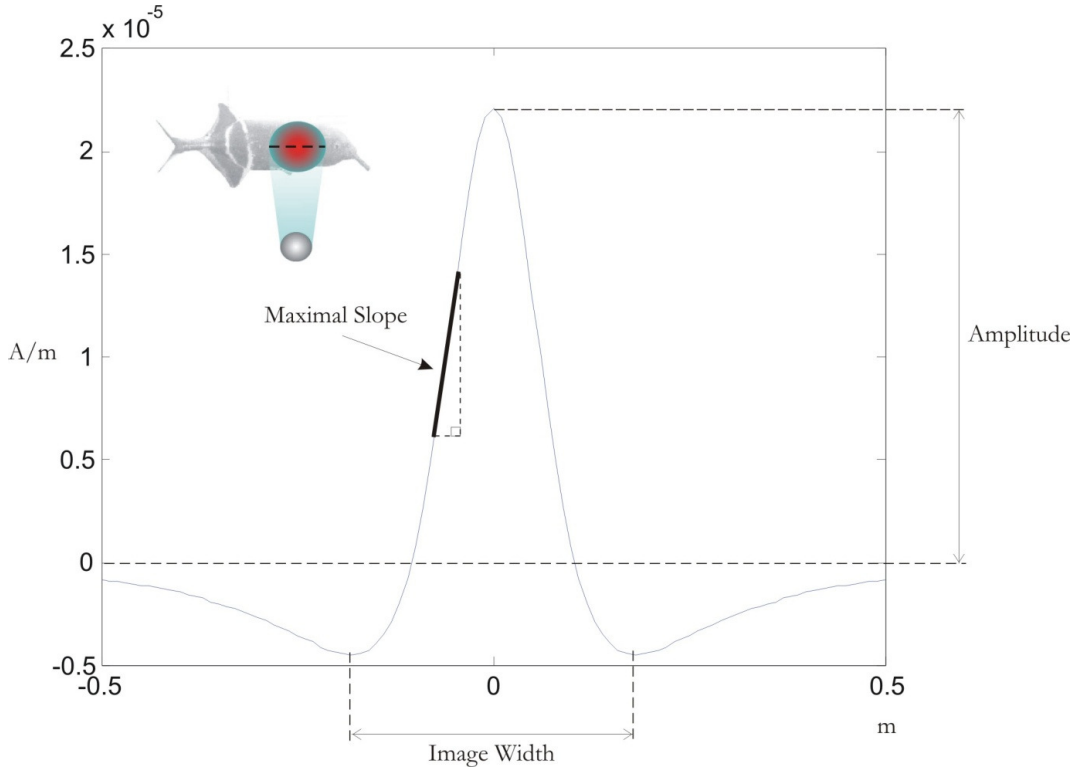

Figure 17 - 2D Cross Section of a Typical Electropotential Pattern

This curve can be uniquely described, as shown in the figure, by three waveform characteristics: the peak amplitude, the image width, and the maximal slope. The image width is measured as the distance between the two ridge peaks and the maximal slope is peak gradient of the curve. Various combinations of these parameters are shown to be directly related to some of the properties of the object that produced the pattern.

3.1.3 Object Location and Range

Assuming a two-dimensional array on the side of the fish, two of the three coordinates of the target position are determined simply by locating the peak of the electropotential pattern on the sensors. The rostrocaudal (head/tail) axis and is analogous to the x axis of the artificial model, and the dorsoventral (fin/belly) is analogous to the z axis.

To locate the object in three-dimensional space, the distance of the object from the EOD source must be known. Experimentation revealed that the peak amplitude and maximal slope are modulated by multiple object properties, so neither can be used alone to determine the distance. Although the peak amplitude and maximal slope are highly correlated when taken as a function of distance, they grow at different rates. It has been found that the quotient of the two quantities does indeed correspond unambiguously to a given object distance (von der Emde 2006). This derived parameter is referred to as the slope-amplitude ratio (SAR).

3.1.4 Object Size and Shape

The total volume of material of a target object contributes, along with other factors, to the amplitude of the electropotential pattern. For a solid sphere, the volume is directly proportional to its radius. Since the distance is the other chief contributor to the amplitude, estimates of the object radius made from the peak amplitude are reasonably accurate when the distance is known. Thus, once the distance is determined from the SAR, it can be used as a calibration factor to find the radius from the peak.

3.1.5 Material Composition

Weakly electric fish have been observed to easily discriminate between highly conductive and highly insulating objects. Metallic objects are rarely seen in the natural environment and the strong electric image they produce is actually irritating or repulsive to the fish. Most objects and materials that are in the intermediate range of conductivity are organic and have complex impedances. WEF are known to determine the capacitive components of such materials by analyzing phase shifts detected by their P-type sensors (see section 1.3.3).

3.2 Sphere Properties vs. Waveform Parameters

In order to develop a forward model that is suitable for inversion, the number of observed waveform characteristics must equal at least the number of desired target properties. Since the relative conductivity will be taken from the polarity and the longitudinal position from the peak location, only the distance and radius need to be identified through an inverse model. Two characteristics of the electric image waveform that vary with the desired properties are the peak electric field and the maximal slope (von der Emde and Schwarz 2000).

3.2.1 Material

The most obvious indicator of the material composition of a target is the polarity of the electric image. The polarity of the image is determined by whether the target is more or less conductive than the medium. Since weakly electric fish are thought to make some distinctions in object permittivity based on phase shifts (Rasnow 1996), analysis of permeability alongside conductivity to distinguish materials requires an oscillating source.

Most objects of interest for artificial electrolocation, however, will fall into one of two categories with respect to conductivity. The majority of metals have a very high conductivity, on the order of 10^7 S/m. Materials such as air, glass, rubber, and wood have very low conductivities, the order of 10^{-15} S/m (Paris and Hurd 1969). The peak electric field due to a sphere near a dipole electric source, as a function of conductivity behaves asymptotically as shown in Figure 18. The field is calculated at 0.1 m from a 1 m, 1 A source where a = 0.05 m and the sphere is 0.5 m from the source. It is evident that there is negligible field variation within the bounds of commonly found metals, and likewise insulators.

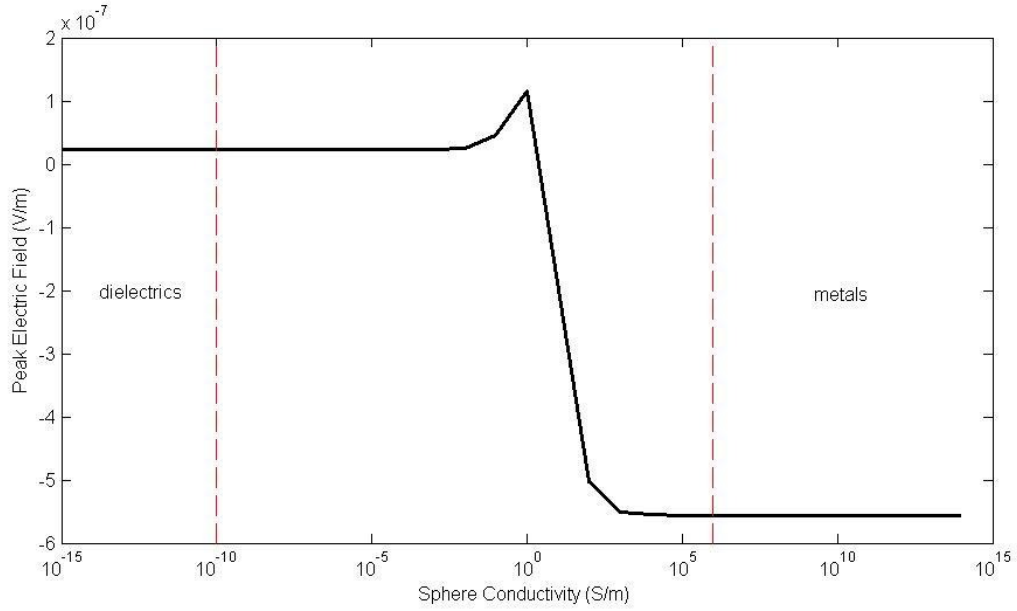

Figure 18 - Sphere Conductivity vs. Peak Electric Field (4.0 S/m medium)

3.2.2 Distance vs. Slope-Amplitude Ratio

Simulations were run using equation 14 to calculate the potential perturbation, via superposition, due to a finite current dipole near a sphere. The electric field component along the measurement line parallel to the dipole was then found by applying the gradient. The slope of this waveform, $\bar{b}$, is then calculated by computing a second gradient. In this paper, a single horizontal accent line over a variable denotes a one-dimensional matrix, a double line a two-dimensional matrix.

$$\bar{b}(y) = \nabla\overline{E_y} \tag{21}$$

The matrices containing the distance and radius ranges of values are defined, respectively, as

$$\bar{d} \stackrel{\text{def}}{=} \langle d_1, d_2, \dots, d_n \rangle \tag{22}$$

$$\bar{a} \stackrel{\text{def}}{=} \langle a_1, a_2, \dots, a_n \rangle \tag{23}$$

From the $\overline{E_y}$ waveform, as shown in Figure 17, the peak amplitude of the electric field, $E_{yp,}$ can be located by determining the position of the three roots of $\bar{b}$ (equation (24)), and choosing the central one (equation(25)) – as the center peak will be higher in magnitude than the ridge peaks for a waveform that is suitable for electrolocation.

$$\{y_{br1}, y_{br2}, y_{br3}\} \stackrel{\text{def}}{=} y \in \bar{b} = 0 \tag{24}$$

$$E_{yp} = \overline{E_y}(y_{br2}) \tag{25}$$

Similarly, another gradient can be applied to $\bar{b}$, whose root will represent the location of the maximal slope of $\overline{E_y}$

$$\{\mathrm{y}_{\nabla \mathrm{b}}\} \stackrel{\text{def}}{=} y \in \overline{\nabla b} = 0 \tag{26}$$

$$b_{max} \stackrel{\text{def}}{=} \bar{b}(\mathrm{y}_{\nabla \mathrm{b}}) \tag{27}$$

The slope-amplitude ratio $R_{b/E}$ is then simply

$$R_{b/E} = \frac{b_{max}}{E_{yp}} \tag{28}$$

The behavior of the SAR with respect to distance is shown in Figure 19, holding a conducting sphere at a constant radius, then varying the distance from a dipolar source.

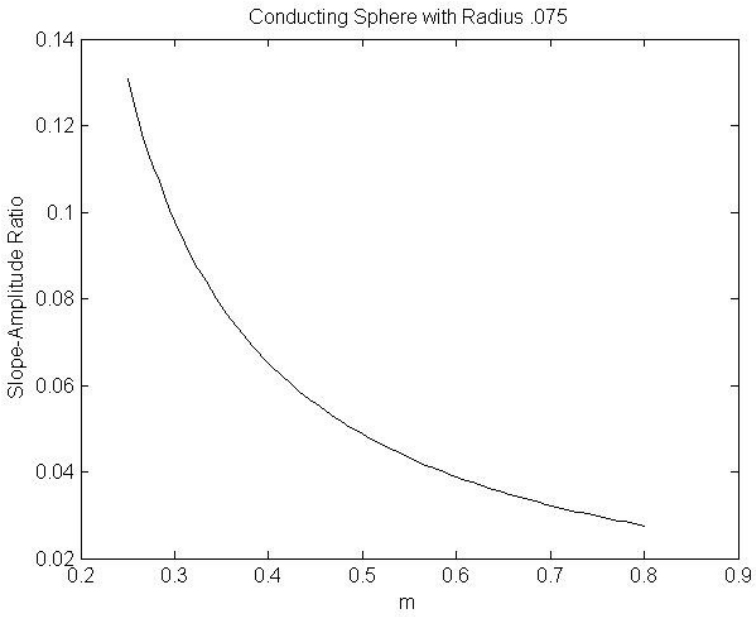

Figure 19 - Distance vs. SAR for a Fixed Radius

Allowing the sphere radius to vary over the pertinent range, however, does not result in a large variation in SAR. This fact is likely why WEF are thought to be able to unambiguously discern distance by using this ratio. It can be seen in Figure 20 that the maximum spread in SAR is approximately 0.01, which is about 7% of the total range. To generate these data, the radius was varied over 100 points between 0.01 and 0.05 m.

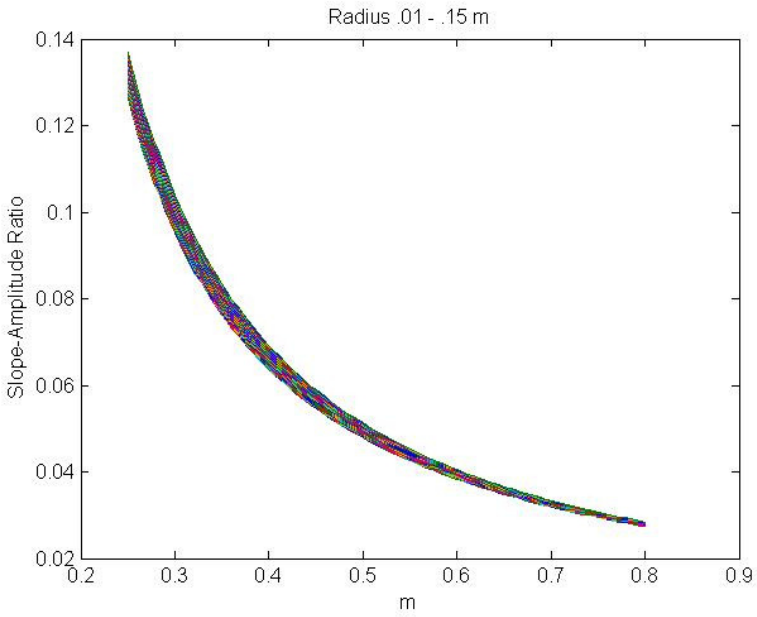

Figure 20 - Distance vs. SAR for a Range of Radii

Note that if a median or average of the above SAR spread is used to remove the radius as an independent variable, then the percent error in $R_{b/E}$ will be at most about half of the spread error ($\approx< 3.5$ %). That maximum error occurs closest to the source, where fidelity is higher. Defining the SAR in terms of the distance, averaged over the radii, thus yields

$$\overline{R_{b/E}}(d) \stackrel{\text{def}}{=} \frac{\sum_{a=a_1}^{a_n} \overline{\overline{R_{\frac{b}{E}}}}(d,a)}{n} \tag{29}$$

3.2.3 Radius vs. Peak Amplitude

Plotting the radius against the peak amplitude E_{yp} at a fixed distance yields the curve shown in Figure 21.

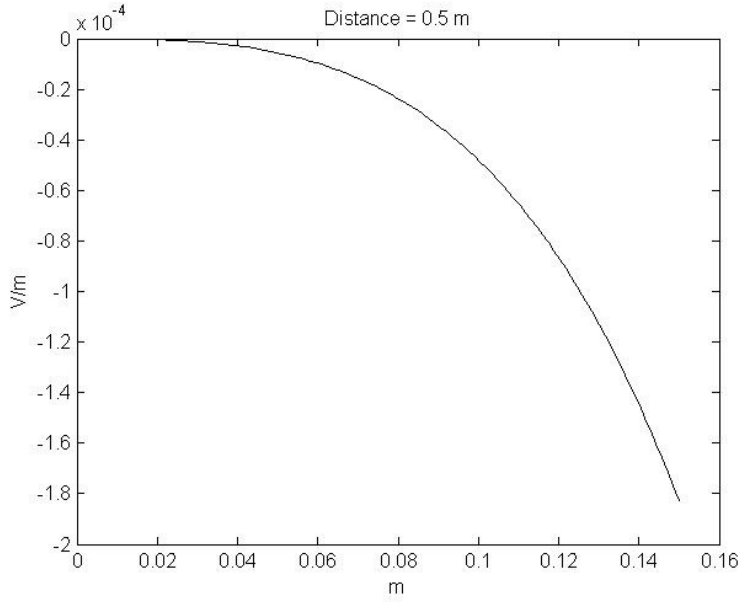

Figure 21 - Radius vs. Peak Amplitude for a Fixed Distance

Unlike the distance and SAR relationship, the peak amplitude is ambiguous with respect to radius because the potential is also significantly modulated by varying source distance. Figure 22 shows the variation in peak amplitude $\overline{E_{yp}}(d, a)$ plotted against the radius for 100 points of distance between 0.15 and 0.8 m.

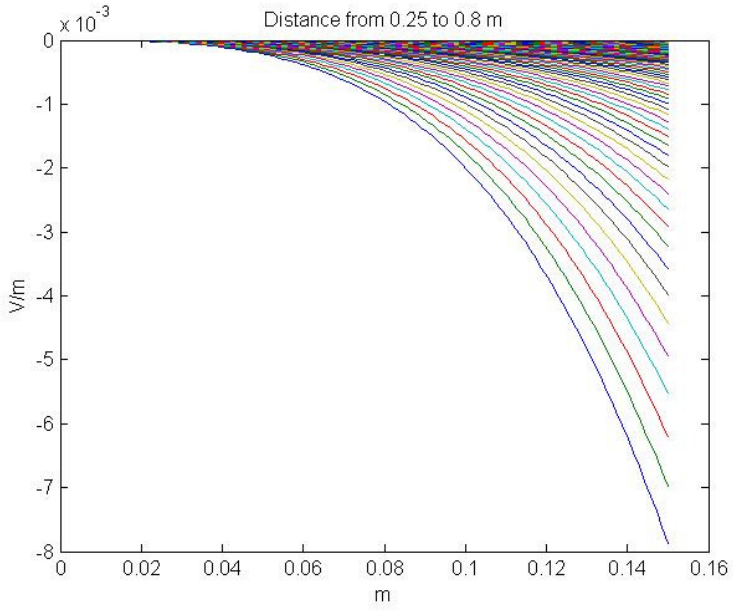

Figure 22 - Radius vs. Peak Amplitude for a Range of Distances

Although the peak amplitude cannot unambiguously reveal the sphere radius, it is clear that distance serves as a calibration factor which, once known (d_0), can reduce E_{yp} to a function of the radius

$$\overline{E_{yp}}(a) \stackrel{\text{def}}{=} \overline{E_{yp}}(d_0, a) \tag{30}$$

3.3 Forward Model

In order to transform the forward model into an inverse model, the relationship must be invertible so as to be simultaneously solvable for radius and distance in terms of peak electric field and slope-amplitude ratio.

$$\begin{matrix} E_{yp} = f(d,a) \\ R_{b/E} = g(d,a) \end{matrix} \Leftrightarrow \begin{matrix} a = F(E_{yp}, R_{b/E}) \\ d = G(E_{yp}, R_{b/E}) \end{matrix} \tag{31}$$

There may be mathematical models that fit the data sufficiently, but they will not necessarily be mathematically invertible. Therefore a matrix manipulation approach was taken. Given the matrix definition of the SAR in equation 29, we can define the relationship between $R_{b/E}$ and *d* in terms of a transformation matrix

$$\overline{R_{b/E}} = \overline{A_R} \cdot \bar{d} \tag{32}$$

where $\overline{A_R}$ is the transformation matrix that maps *d* onto $R_{b/E}$. Similarly, the peak amplitude given a calibration distance d_0 can be written in terms of the radius matrix as

$$\overline{E_{yp}} = \overline{A_E} \cdot \bar{a}; d = d_0 \tag{33}$$

where $\overline{A_E}$ is the transformation matrix that maps *d* onto $R_{b/E}$.

Equations (32) and (33) comprise the forward electrolocation model. The transformation matrices $\overline{A_R}$ and $\overline{A_E}$ will be unique to each set of parameters that describe the source and medium. Since these parameters would be known in advance of an electrolocation task, the matrices can be used to construct an inverse model that is appropriate for the intended environment. The next chapter derives the inverse model through matrix-algebraic manipulation then tests its validity by introducing independent inputs.

4 Inverse Electrolocation Model

The purpose of the inverse electrolocation model is to provide an estimate of the distance, radius, and conductive polarity of a target sphere, given the electric field perturbation generated by the sphere's presence. The forward model in section 3.1 related the characteristics of a sphere to certain parameters of its electrosensory pattern in matrix algebra form. Operations on the transformation matrices yield the desired inverse relationship.

Once the inverse model is derived, one need only know the peak amplitude and maximal slope of a measured sphere signature to make approximations of the sphere size, location, and relative electric polarity. Since physical measurements were not in the scope of this work, FEM models of spheres were generated to provide independent input to the predictor. Simulations were performed for conducting and insulating spheres of varying size and location.

4.1 Rearranging Variables

4.1.1 Distance vs. Slope-Amplitude Ratio

Given the matrix definition of the SAR in equation 32, the transformation matrix $\overline{A_R}$ is found by division:

$$\overline{A_R} = \frac{\overline{R_{b/E}}}{\bar{d}} = \langle \mathrm{A_{R1}}, \mathrm{A_{R2}}, \dots, \mathrm{A_{Rn}} \rangle \tag{34}$$

Before the transformation matrix can be inverted it must be converted into a diagonal matrix (two-dimensional matrices are denoted by the double-line accents overhead) by multiplying the identity matrix $\overline{\overline{\mathrm{I}}}$

$$\overline{\overline{\mathrm{I}_{\mathrm{n}}}} \stackrel{\text{def}}{=} \begin{bmatrix} 1 & 0 & \cdots & 0 \\ 0 & 1 & \cdots & 0 \\ \vdots & \vdots & \ddots & \vdots \\ 0 & 0 & \ldots & 1 \end{bmatrix} \tag{35}$$

$$\overline{\overline{A_R}} = \overline{A_R} \cdot \overline{\overline{\mathrm{I}_{\mathrm{n}}}} = \begin{bmatrix} \mathrm{A_{R1}} & 0 & \cdots & 0 \\ 0 & \mathrm{A_{R2}} & \cdots & 0 \\ \vdots & \vdots & \ddots & \vdots \\ 0 & 0 & \ldots & \mathrm{A_{Rn}} \end{bmatrix} \tag{36}$$

The inverse transformation matrix is given by

$$\overline{\overline{A_R}}^{-1} = \frac{1}{\left|\overline{\overline{A_R}}\right|} \cdot \overline{\overline{C_n}} \tag{37}$$

where $\left|\overline{\overline{A_R}}\right|$ is the determinant of $\overline{\overline{A_R}}$ and $\overline{\overline{C_n}}$ is a matrix of cofactors whose form is dependent on the size of $\overline{\overline{A_R}}$. Finally, the SAR can be mapped onto a distance matrix using the inverse transform

$$\overline{d\left(R_{b/E}\right)} = \overline{\overline{A_R}}^{-1} \cdot \overline{R_{b/E}} \tag{38}$$

4.1.2 Radius vs. Distance-Calibrated Peak Amplitude

The peak amplitude can only yield a radius once the distance to the target has been estimated. Initially, $\overline{\overline{E_{yp}}}$ is a two-dimensional matrix dependant on both $\bar{d}$ and $\bar{a}$. However, $\overline{\overline{E_{yp}}}$ can be viewed as a concatenation of one-dimensional vectors giving $\overline{E_{yp}}(a)$ for each given *d*:

$$\overline{\overline{E_{yp}}}(d,a) = \begin{bmatrix} \overline{E_{yp}}\,(d_1,a) \\ \overline{E_{yp}}(d_2,a) \\ \vdots \\ \overline{E_{yp}}(d_n,a) \end{bmatrix} \tag{39}$$

The appropriate peak amplitude matrix, calibrated by the distance estimate d_0, is selected from the rows of $\overline{\overline{E_{yp}}}(d,a)$, each of which have their own radius transformation matrix as defined in equation 33. Dividing to solve for the transformation matrix yields:

$$\overline{A_{E,d}} = \frac{\overline{\overline{E_{yp}}}(d_0,a)}{\bar{a}} \tag{40}$$

The inverse relation mapping the peak amplitude onto the radius is thus:

$$\bar{a}\left(E_{yp}\right) = \overline{\overline{A_{E,d}}}^{-1} \cdot \overline{E_{yp}} \tag{41}$$

4.2 Simulation Procedure

Numerical validation of the method of images formulation of point current sources near spheres in conducting media (section 2.1) was performed using FEM. Electric fields computed with a model were sufficiently close to the method of images calculations so as to provide reasonable confidence in both methodologies. The purpose of the FEM sphere model was to create independent inputs to the inverse electrolocation simulation, so that the fields being combined with the inverse transformation matrices were not the same ones used to construct them.

4.2.1 Preparation of Matrices

Before simulation data can be analyzed, the transformation matrices appropriate for the given assumptions of the simulation must be constructed from the field equations and parametric relationships. The assumptions used for the simulation are for that of a small, mobile electrolocation apparatus in an unbounded marine environment. Table 1 shows the chosen constants and constraints.

Table 1 - Simulation Constraints

Parameter	Variable	Value/Range
dipole length	L	1 m
source strength	I	$\pm$ 1 A
medium conductivity	σ_1	4 S/m
sphere conductivity	σ_2	1E-5, 1E5 S/m
sphere radius	a	0.01 – 0.15 m
radius resolution	-	.0014 m
sphere distance from source	d	0.25 – 0.8 m
distance resolution	-	.0055 m
measurement line resolution	-	0.01 m

The given parameters in Table 1 were inserted into a MATLAB script that varied the distance and radius over the given resolutions to create the associated SAR and peak amplitude matrices. All matrices were then interpolated to provide intermediate values and the inverse transformation matrices were calculated according to the procedure outlined in section 0. The script created two unique sets of matrices, one each for the insulating and conducting sphere cases.

4.2.2 FEM Model Simulations

Models of varying sphere size and location were created using the Vector Fields OPERA modeler. The medium (4 S/m) was extended to 10 m in each direction from the origin to approximate an unbounded region. The electric field perturbation along the measurement line was computed by subtracting the fields due to the source from the total fields to obtain only the scattered fields produced by each sphere. Eighteen models in all were computed, as per varying the sphere conductivity, radius, and location as shown in Table 2.

Table 2 - FEM Model Parameters

Parameter	Variable	Value/Range
sphere conductivity	σ_2	1E-5, 1E5 S/m
sphere radius	a	0.025, 0.075, 0.125 m
sphere distance from source	d	0.25, 0.5, 0.75 m

Each FEM model produced a one-dimensional matrix representing the computed values of $\tilde{E}_y$ along the designated measurement line. This matrix was run through a smoothing algorithm to aid in slope computation. The peak amplitude and SAR were then calculated according to the procedure outlined in section 3.2.2. These two values were the only data passed to the inverse electrolocation algorithm from the FEM simulation.

4.3 FEM Simulation Results

Results from the conducting sphere and insulating sphere simulations are given in Table 3 and Table 4, respectively. In all cases the spheres were successfully identified by their peak amplitude polarity as conducting or insulating. The data were then applied to the appropriate transform matrices.

Table 3 - Simulation Results for Conducting Spheres

Distance			Radius		
Actual (m)	Predicted (m)	% error	Actual (m)	Predicted (m)	% error
0.25	*0.2638*	-5.52%	0.025	*0.0278*	-11.20%
0.25	*0.2611*	-4.44%	0.075	*0.081*	-8.00%
0.25	*0.2569*	-2.76%	0.125	*0.1295*	-3.60%
0.5	*0.5183*	-3.66%	0.025	*0.0272*	-8.80%
0.5	*0.5037*	-0.74%	0.075	*0.0761*	-1.47%
0.5	*0.4948*	1.04%	0.125	*0.122*	2.40%
0.75	*0.2993**	60.09%	0.025	*0.01**	60.00%
0.75	*0.6429*	14.28%	0.075	*0.0568*	24.27%
0.75	*0.7124*	5.01%	0.125	*0.1136*	9.12%

*computed field values were numerically noisy due to finite element limitations for very small spheres at larger distances

Table 4 - Simulation Results for Insulating Spheres

Distance			Radius		
Actual (m)	Predicted (m)	% error	Actual (m)	Predicted (m)	% error
0.25	*0.2572*	-2.88%	0.025	*0.0268*	-7.20%
0.25	*0.2538*	-1.52%	0.075	*0.0783*	-4.40%
0.25	*0.25*	0.00%	0.125	*0.1281*	-2.48%
0.5	*0.4985*	0.30%	0.025	*0.0251*	-0.40%
0.5	*0.4926*	1.48%	0.075	*0.0742*	1.07%
0.5	*0.4804*	3.92%	0.125	*0.119*	4.80%
0.75	*0.6933*	7.56%	0.025	*0.0218*	12.80%
0.75	*0.7314*	2.48%	0.075	*0.0726*	3.20%
0.75	*0.6818*	9.09%	0.125	*0.1072*	14.24%

Generally, it can be seen in the above tables that the predictions were more accurate when the spheres were larger and closer to the source. The implications of the results and further conclusions are discussed in the following chapter.

5 Discussion and Conclusions

The simulation results from the previous chapter show that for a range of target sizes and distances, artificial underwater electrolocation is achievable through the mathematical models derived in this dissertation. This preliminary result sets the stage for further investigations as outlined in this chapter.

It is important to identify the sources of error, as done below, between the predictions and ground truth so that they might be mitigated in future work. The estimated minimum range of detection for varying source lengths and amplitudes is given. Suggestions for future work include further validation through physical experimentation and expansion of the model to multipoles in three-layer media.

5.1 Sources of Error

Although the method of images is an exact solution due to the uniqueness theorem (Jackson 1999), the integrals contained in the formulas for the potential perturbation do not have a closed-form solution and must be treated numerically. Thus any models derived from these formulas contain the error inherent in numerical approximation. The integrations performed in MATLAB used a vectorized quadrature routine. As explained in section 3.2.2, the ambiguity of viewing the slope-amplitude ratio as a unique function of distance is eliminated by averaging the matrices across all values of the radius to produce a single one-dimensional transform. This averaging will result in predictable errors that are more pronounced for distances close to the source.

The measurement line waveforms produced by the FEM simulations are only as precise as the limited finite element mesh will allow. Often, a mesh that is sufficiently fine to capture very small field variations will produce a model that is too large to successfully run on a given

computing platform. Referring to Table 3, the model for the 0.025 m diameter sphere at a distance of 0.75 m produced a peak amplitude field perturbation on the order of 1×10^{-7} V/m. This value was at the lower limit of what the mesh could accommodate, resulting in a "noisy" signature that produced a large error.

5.2 Source Magnitude and Detection Range

Electroreceptive animals that live in seawater environments have a minimum electric field detection threshold on the order of 1×10^{-6} V/m (Peters, Eeuwes and Bretschneider 2007). This value is consistent with measured EM background noise levels in marine regions (Kraichman 1977). Using this value as a benchmark, the effective electrolocation range for a given source strength and configuration can be found. Since the target size also affects the field amplitude, it must be held constant.

Assuming a conducting target sphere with a radius of one tenth the dipole length L, the contour corresponding to a 1×10^{-6} V/m peak amplitude is plotted against the sphere distance and dipole length in Figure 23. The implication of this plot is that in order for a conducting target of size equal to one tenth the length of the dipole source to be detectable at a distance equal to half the length of the dipole, at least ±100 A of current is needed. It is important to note that there may be practical issues and trade-offs with regard to using very high levels of current in a marine volume.

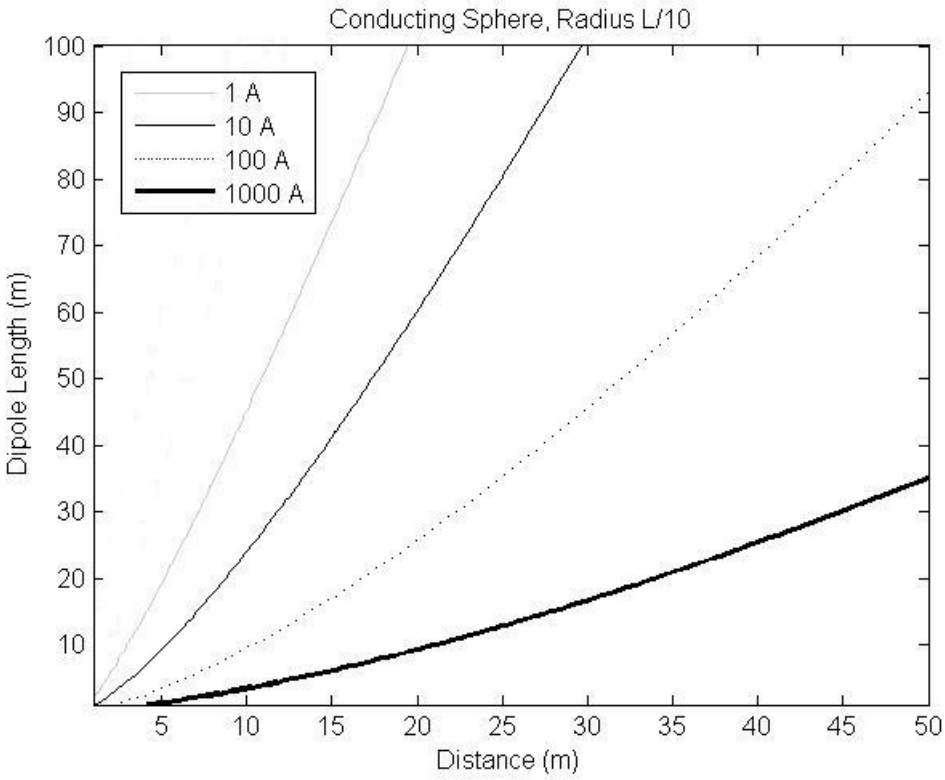

Figure 23 - Detection Range for Conducting Spheres

As seen in Table 3 and Table 4 in section 4.3, the insulating spheres can be accurately detected at a further distance than the conducting spheres. Thus, Figure 23 represents the minimum detection range for a given scenario. Keeping the dipole length constant at 1 m, the detection range can be viewed as the radius, distance, and source magnitude are varied. Figure 24 plots the contour of the 1×10^{-6} V/m minimum threshold for conducting spheres against both target distance and radius.

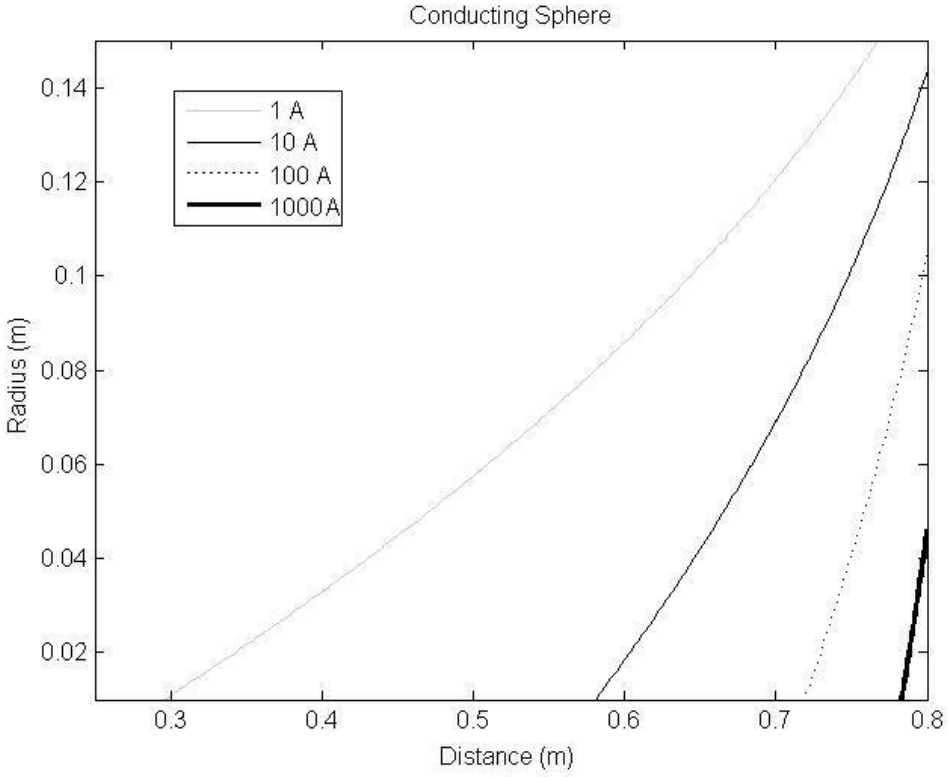

Figure 24 - Detection Range of a 1 m Source for Conducting Spheres

5.3 Future Efforts

Employing the method of images, instead of uniform or point-dipole approximations, to characterize the dipole source will allow more detailed modeling of the fields surrounding an electrolocation vehicle or apparatus. The use of source images will also allow the model to be refined to account for the three-layer media of a littoral region. Since the images include linear current distributions, the line images would have to be redefined as a sum of multiple point sources, or image theory for line distributions could be applied.

Weakly electric fish have been observed to discriminate object shapes and organic material with capacitive components. Identification of spheroids and discs would be particularly

useful in artificial electrolocation. Further, the use of low-frequency oscillating discharge signals to obtain phase information could aid in target characterization.

Further verification of the methods outlined in this work would be best achieved with physical measurements. A setup consisting of a linear array of electropotential sensors immersed in water (of appropriate conductivity) with various test spheres and a simple dipolar current source would provide initial confirmation of the model's validity. Further experiments should be conducted with two-dimensional sensor arrays of varying sensor resolution.

5.4 Conclusion

The peculiar animals that inspired this study and other parallel investigations are but a few in a long line of natural phenomena that have led to technological innovations. Weakly electric fish – like their acoustic counterparts, dolphins – have best shown us how to view the environments in which they reside. The biologically inspired task of electrolocation can serve as a stealthier alternative or complementary methodology to the more common undersea acoustic detection. Application of the method of images and the principal of duality produces a flexible and accurate mathematical model of a finite dipolar current source near conducting spheres in conducting media. The field perturbations caused by the introduction of material objects to the media are directly related to the properties of the objects.

The known relationships between a sphere's parameters and the characteristics of its electrosensory pattern inform a forward model that is inverted using matrix manipulation. Simulations of the inverse model, using as input the electrosensory patterns from finite element model of spheres, revealed that artificial underwater electrolocation can be achieved with reasonable accuracy. Performance and detection range can be increased by adjusting the current

source intensity within the physical constraints of the apparatus and environment. Validation of the model through physical measurements and expansion of the model to multipoles in layered media is recommended.

Appendix I – Derivation of Potential Perturbation by the Method of Images

Reproduced with permission from (W. T. Norris 2010), the potential perturbation due to the Kelvin image is

$$\breve{\Phi}_{\varepsilon,\mathrm{k}} = -\frac{\mathrm{q}\gamma}{4\pi\varepsilon_0\varepsilon_1}\frac{\mathrm{r_i}}{\mathrm{a}}\frac{1}{\mathrm{d}} \tag{42}$$

where

$$d = \sqrt{r_s^2 + r_i^2 - 2rr_i cos(\theta)} \tag{43}$$

The potential perturbation due to the distributed image is:

$$\breve{\Phi}_{\varepsilon,\mathrm{d}} = -\frac{\mathrm{q}\gamma}{4\pi\varepsilon_0\varepsilon_1}\frac{1}{\mathrm{a}}\int_0^{r_i}\frac{(1-\gamma)}{2}\frac{\left(\frac{X}{r_i}\right)^{-(1+\gamma)/2}}{\sqrt{r_s^2 + X^2 - 2rXcos(\theta)}}\,dX \tag{44}$$

Using integration-by-parts:

$$\frac{\mathrm{q}\gamma}{4\pi\varepsilon_0\varepsilon_1}\frac{1}{\mathrm{a}}\frac{r_i}{\sqrt{r_s^2 + r_i^2 - 2rr_i cos(\theta)}} + \frac{\mathrm{q}\gamma}{4\pi\varepsilon_0\varepsilon_1}\frac{1}{\mathrm{a}}\int_0^{r_i}\frac{(1-\gamma)}{2}\frac{\left(\frac{X}{r_i}\right)^{-(1+\gamma)/2}}{\sqrt{r_s^2 + X^2 - 2rXcos(\theta)}}\,dX \tag{45}$$

Superposition of the two images yields

$$\breve{\Phi}_{\varepsilon} = \breve{\Phi}_{\varepsilon,k} + \breve{\Phi}_{\varepsilon,d} = \frac{q\gamma}{4\pi\varepsilon_0\varepsilon_1}\frac{1}{a}\int_0^{r_i}\frac{(1-\gamma)}{2}\frac{\left(\frac{X}{r_i}\right)^{-(1+\gamma)/2}}{\sqrt{r_s^2 + X^2 - 2rXcos(\theta)}}\,dX \tag{46}$$

Appendix II – Duality and Method of Images FEM Validation

The electric potential Φ in standard electrostatics due to a point charge is well-known and given by (Jackson 1999):

$$\Phi = \frac{1}{4\pi\varepsilon}\frac{q}{|\overrightarrow{r}|} \tag{47}$$

where ε is the electric permittivity of the medium ($\varepsilon = \varepsilon_0\varepsilon_r$, where ε_0 is the permittivity of free space and ε_r is the relative permittivity of the medium), q is the source charge and the vector r points to the field location.

According to the duality described in section 2.1.3, the electric potential due to a point current source is thus given by:

$$\Phi = \frac{1}{4\pi\sigma}\frac{I}{|\overrightarrow{r}|} \tag{48}$$

where σ is the electric conductivity of the medium and I is the point source current. Although, equation 48 is a known relation (Linck 2002), it is compared to a numerical current source model as further validation of duality. The Vector Fields OPERA finite element method (FEM) software suite was used to model a current source in a conducting medium. Since point sources

are unavailable in the software, the source was modeled as a small sphere of radius 0.0025 m with a voltage boundary condition to affect a 1 A current in the medium. The medium was assigned a nominal seawater conductivity of 4 S/m and extended 11 m in each dimension to minimize reflections. The potential was measured along a line extending from the source along 100 data points to 1 m and compared to the analytically calculated falloff, shown in Figure 25, as implemented in MATLAB.

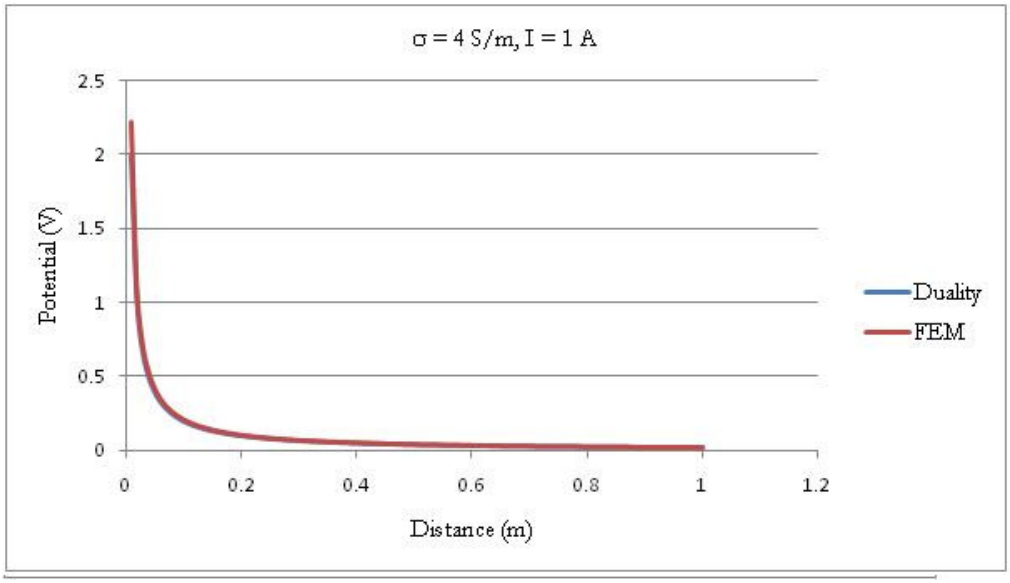

Figure 25 - Electric Potential Falloff of a Point Current Source in Seawater

Figure 26 shows the comparison of the E_y field signature, computed using the method of images and FEM techniques, for a 1 m dipole source near a sphere.

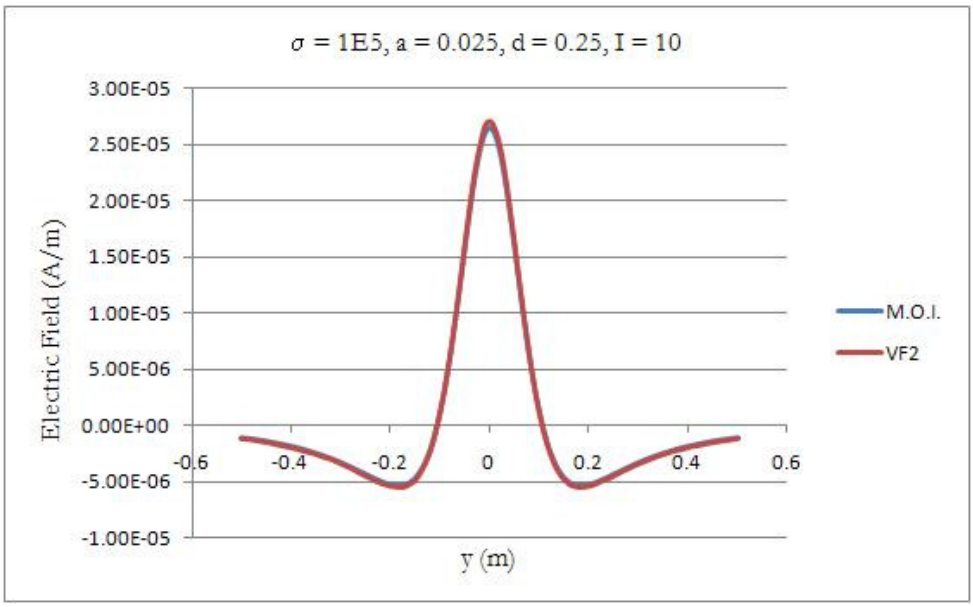

Figure 26 - Sphere Signature, Method of Images vs. FEM

Bibliography

Arizzi, Rocco. "Applications of Artificial Underwater Electrolocation." *Military Sensing Symposium: Battlespace Acoustic, Magnetic and Seismic Sensing.* SENSIAC, 2009.

Babineau, D., A. Longtin, and J.E. Lewis. "Modeling The Electric Field Of Weakly Electric Fish." *The Journal of Experimental Biology 209*, 2006: 3636-3651.

Bass, A.H. "Electric organs revisited." In *Electroreception*, by T.H. Bullock and W. Heiligenberg, 13–70. New York: Wiley, 1986.

Bronzino, R. In *Introduction to Biomedical Engineering*, 8-4. CRC Press, 1999.

Chetty, G., and A. Russell. "Electric Field based Sensing for Underwater Vehicle Guidance." *2nd Intemational Conference on Bioelectromagnetism.* Melbourne, Australia, 1998.

Darwin, Charles. *On the Origin of Species.* 1859.

Elliott, Robert S. *Electromagnetics: History, Theory, and Applications.* New York: Wiley-IEEE Press, 1999.

Federation of American Scientists. *Introduction to Naval Weapons Engineering Syllabus, Sonar Propagation.* 2009. http://www.fas.org/man/dod-101/navy/docs/es310/SNR_PROP/snr_prop.htm.

Hartmann, Gregory K. *Weapons That Wait .* Annapolis, MD: Naval Institute Press, 1979.

Heiligenberg, Walter. "Coding and Processing Of Electrosensory Information in Gymnotiform Fish." *J. exp. Biol. 146*, 1989: 255-275.

Jackson, John David. *Classical Electrodynamics (3rd ed.).* New York: Wiley, 1999.

Knudsen, Eric I. "Spatial Aspects of the Electric Fields Generated by Weakly Electric Fish." *J. comp. Physiol. 99*, 1975: 103--118.

Kraichman, M.B. *Electromagnetic Background Noise in The Ocean Due to Geomagnetic Activity in the Period Range 0.5 to 1000 seconds.* NSWC/WDL/TR 77-41, Silver Spring, MD: Naval Surface Weapons Center, White Oak Laboratory, 1977.

Kraichman, M.B. *Handbook Of Electromagnetic Propagation In Conducting Media.* U.S. Government Printing Office, 1970.

Linck, Jessica E. *Mathematical Model of the Shallow Water Static Electric Field Signatures of Naval Vessels, NSWCCD-TR-2002/01.* West Bethesda, MD: Naval Surface Warfare Center, Carderock Division, 2002.

Lissman, H.W. *On the Function and Evolution of Electric Organs in Fish.* Cambridge, U.K.: Department of Zoology, University of Cambridge, 1957.

Lissman, H.W., and K. E. Machin. *The Mechanism Of Object Location In Gymnarchus Niloticus And Similar Fish.* Cambridge, U.K.: Department of Zoology, University of Cambridge, 1958.

Maciver, A Malcolm, and E Mark Nelson. "Sensory Acquisition In Active Sensing Systems." *Journal of Comparative Physiology*, 2006: 192: 573–586.

MacIver, Malcolm A., and Mark E. Nelson. "Towards a Biorobotic Electrosensory System." *Autonomous Robots 11*, 2001: 263–266.

Norris, W. T. *Field due to the Charge Induced on a Dielectric Sphere by an External Charge.* Birmingham, UK: Aston University, 2010.

Norris, W.T. "Charge Images in a Dielectric Sphere." *IEEE Proceedings on Scientific Measurement Technology, Vol. 142, No. 2.* 1995. 142 - 150.

NSWCCD Signatures Directorate. *Submarine Electromagnetics Tutorial.* NSWCCD-TR-2002/12, West Bethesda, MD: Naval Surface Warfare Center, Carderock Division, 2003.

Paris, D. T., and F. K. Hurd. *Basic Electromagnetic Theory.* New York: McGraw Hill, 1969.

Peters, R.C., L.B.M. Eeuwes, and F. Bretschneider. "On the Electrodetection Threshold of Aquatic Vertebrates with Ampullary or Mucous Gland Electroreceptor Organs." *Biol. Rev. 82*, 2007: 361–373.

Pettigrew, John D. "Electroreception in monotremes." *The Journal of Experimental Biology 202*, 1999: 1447–1454.

Purpura, J.W., W.M. Wynn, and P.J. Carroll. "Assessment of an Active Electromagnetic Sensor for Hunting Buried Naval Mines." *OCEANS '04. MTTS/IEEE TECHNO-OCEAN '04 .* IEEE, 2004.

Rasnow, Brian. *The Effects of Simple Objects on the Electric Field of Apteronotus.* Pasadena, CA: Division of Biology, California Institute of Technology, 1996.

Rhodes, Mark. "Electromagnetic Propagation in Sea Water and its Value in Military Systems." *Systems Engineering For Autonomous Systems 2007 Conference Proceedings.* 2007.

Solberg, J. R., K. M. Lynch, and M.A. McIver. *Active Electrolocation for Underwater Target Localization.* Evanston, IL: Northwestern University, 2008.

von der Emde, G. "Non-visual Environmental Imaging and Object Detection Through Active Electrolocation in Weakly Electric Fish." *Journal of Comparative Physiology A*, 2006.

von der Emde, G., and S. Schwarz. *Three-Dimensional Analysis of Object Properties during Active Electrolocation in Mormyrid Weakly Electric Fishes (Gnathonemus Petersii).* Bonn, Germany: Institut fur Zoologie, Universitat Bonn, 2000.